

## RESEARCH ARTICLE

# Grid Connection Using a Structure That Combines a Buck Converter and a Push-Pull Converter to Reduce the Low-Frequency Current Ripple of the Fuel-Cell

GYOUNG-JONG SON<sup>1</sup>, FEEL-SOON KANG<sup>2</sup>, (Member, IEEE), AND SUNG-JUN PARK<sup>1</sup>

<sup>1</sup>Department of Electrical Engineering, Chonnam National University, Gwangju 61186, South Korea

<sup>2</sup>Department of Mechatronics Engineering, Gyeongsang National University, Jinju 52725, South Korea

Corresponding author: Feel-Soon Kang (feelsoon@gnu.ac.kr)

This work was supported by the fund of research promotion program, Gyeongsang National University, 2022.


**ABSTRACT** In a grid-connected power generation system using a fuel cell, the low-frequency ripple component must be maintained within an allowable range to improve the lifespan and efficiency of the fuel cell. We propose a grid connection method using a structure that can reduce the low-frequency ripple component of the fuel cell output current by combining a buck converter and a push-pull converter. The proposed converter has a structure in which the inductor of the non-isolated dc-to-dc converter and the current source inductor are shared. Although it is a two-stage structure, it has the same number of inductors as the single-stage method, and the capacitor, an intermediate voltage source, can be removed. The high-frequency transformer is designed so that the rated output is possible even at the lowest output value of the fuel cell. The current peak value of the push-pull converter is reduced by operating the buck converter's switching frequency at twice the push-pull converter's switching frequency. The operation mode of the proposed converter and the controller design method will be described in detail. A grid-connected inverter is constructed using the proposed converter, and the feasibility of the proposed approach is verified through simulations and experiments on a 1kW prototype.

**INDEX TERMS** Converter, fuel-cell, grid-connected, inverters, push-pull, total harmonic distortion (THD), zero voltage switching (ZVS).

## I. INTRODUCTION

Power generated in the unit cell of a fuel cell is usually in the form of a low voltage and a large current. Many cells are stacked in series in a fuel cell to increase the output voltage, but a dc voltage suitable for grid connection requires a step-up using a dc-dc converter. To efficiently connect the power generated from the fuel cell system to the grid, the power converter for fuel cells requires the following conditions [1], [2], [3], [4], [5], [6], [7], [8], [9], [10].

- 1) Controllable the input power of the fuel cell according to the command value

The associate editor coordinating the review of this manuscript and approving it for publication was Zhilei Yao .

- 2) high-power factor and low THD for the grid current when connecting to the grid
- 3) high efficiency for a high boosting ratio and voltage fluctuation rate
- 4) allowable low-frequency ripple component of the fuel cell current.

In a grid-connected power generation system using a fuel cell, the grid voltage ripple can cause a low-frequency ripple component in the fuel cell output current [4], [11], [12]. To increase the fuel cell's efficiency and lifespan, the low-frequency ripple (100~120Hz) is limited to 15% of the output of the fuel cell, and the 50~60Hz ripple component is limited to within 10% at 10~100% load [8]. A significant output filter capacitor can reduce low-frequency current ripple,

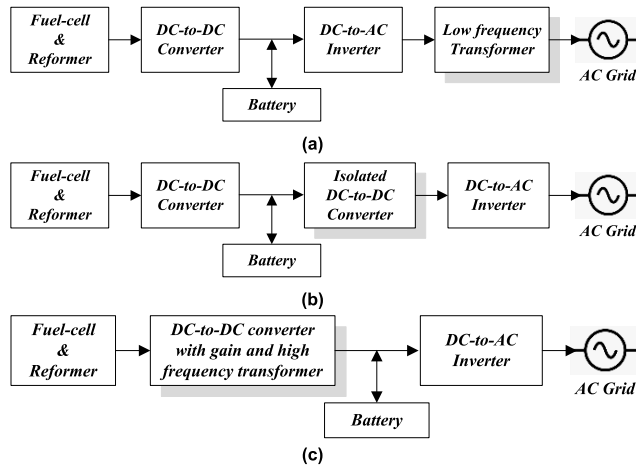


**FIGURE 1.** Grid connection method of fuel cell system, (a) method using a low-frequency transformer, (b) method using converter having high-frequency transformer, (c) method using single-stage converter having high-frequency transformer.

but it increases the volume and weight of the power generation system [5], [13]. In order to reduce the low-frequency ripple component to an acceptable level, a method to improve the control strategy [5], [6], [14] and a method to add a hardware circuit are introduced [7], [15], [16].

Power conversion systems for fuel cells for grid connection can be classified according to galvanic isolation and boosting methods between fuel cells and the grid [9], [17], [18], [19], [20], [21], [22], [23], [24], [25], [26], [27]. There is a method of isolating and boosting the 25–45V of the fuel cell and grid voltage using a low-frequency transformer and a way of insulating and boosting the grid and fuel cell voltage using an isolated dc-to-dc converter employing a high-frequency transformer.

Fig. 1(a) shows a block diagram of a grid-connected inverter for fuel cells using a low-frequency transformer [28], [29]. In general, the output voltage of a 1kw fuel cell is DC 29~60V and boosted to DC 350~400V using a boost converter. The output voltage of the boosted converter is converted to AC 110V or 220V using a single-phase full-bridge dc-to-ac PWM (Pulse width modulation) inverter. The converted AC voltage is connected to the grid using a low-frequency transformer. Here, the battery supplies power to the fuel cell system during the initial start-up. When the fuel cell system starts and generates power, the battery is charged using the generated voltage for the following initial start-up. In Fig. 1(a), the overall system efficiency is the product of the efficiency of each power converter, so it is not easy to increase the overall efficiency. In addition, the grid-connected inverter for fuel cells has a large current and low-efficiency characteristics because the power generation voltage of the fuel cell is lower than the grid-connected voltage. In particular, since a low-frequency transformer is used, the overall weight and size of the inverter increase, and the manufacturing cost increases.

Fig. 1(b) shows a block diagram of a grid-connected inverter for fuel cells using a high-frequency transformer.

In the case of a grid-connected inverter for fuel cells using a high-frequency transformer, compared to the existing grid-connected inverters for fuel cells using a low-frequency transformer, the weight and size can be reduced, and the manufacturing cost is lowered. However, the high-frequency transformer has a problem of poor stability because it is possible to induce dc offset voltage as a grid power source. Moreover, the control is complicated, and the efficiency is lowered by adding an isolated dc-to-dc converter [17], [18], [19], [20], [21], [22], [23], [24], [25], [26], [27].

Fig. 1(c) shows the block diagram of the improved fuel cell grid-connected inverter using the existing high-frequency transformer. It is a single-stage method that increases the high-frequency transformer's step-up ratio instead of eliminating the dc-to-dc converter for step-up [28], [29], [30], [31], [32], [33], [34], [35], [36].

The fuel cell has a characteristic of a low voltage and high current due to a low cell voltage. To use the low voltage generated by the fuel cell as commercial power, a power converter in which a boost converter and an inverter are combined is essential [3], [4], [5], [6], [7], [8], [9], [10]. In particular, it is difficult to satisfy the efficiency and performance required by the overall system with the general dc-to-dc converter technology due to the fuel cell's low voltage and high current characteristics, the significant voltage fluctuation characteristics according to the load, and the high step-up ratio. A general push-pull converter has a limited range of use due to the voltage stress of the switching device. However, the push-pull converter has a structure suitable for power converters that require variable low-voltage to high-voltage output, such as fuel cells [44], [46], [47].

This paper proposes a power converter structure capable of ZVS (Zero voltage switching) and ZCS (Zero current switching) in a fuel cell. The proposed push-pull converter realizes ZVS or ZCS by a passive clamp circuit and solves the immediate overvoltage problem of the push-pull converter. In addition, by synchronizing the switching signal of the buck converter with the double frequency to the switching signal of the push-pull converter, the peak current of the inductor and the transformer winding is reduced. The proposed converter is a two-stage converter, but unlike the existing two-stage method, there is no voltage filtering capacitor between the power conversion stages. Compared to the single-stage technique, only one switching device is added.

A fuel cell uses a battery as initial starting power and a separate dc-to-dc converter as control power. Therefore, it needs to replace the battery after a specific period is necessary or configure the charger using another separate dc-to-dc converter. To solve the problem, a method of directly charging a battery in a fuel cell is proposed using the relationship between the fuel cell voltage and the amount of oxygen in the fuel cell system. This method uses the fuel cell's low voltage and high current characteristics for battery charging to improve performance and efficiency.

**II. PROPOSED FUEL-CELL-POWERED CONVERTER INTEGRATING BUCK CONVERTER AND PUSH-PULL CONVERTER**

**A. COMPARISON OF DC-TO-DC CONVERTER TOPOLOGIES USED FOR FUEL CELL POWER GENERATION**

The output voltage fluctuation range in fuel cells is more than doubled according to the output current. In addition, fuel cells have low voltage and significant current characteristics, so a high step-up ratio and galvanic isolation are essential for the grid connection. Fig. 2 shows various power converters applied as dc-to-dc converters for fuel cells. Fig. 2(a) is a commonly used full-bridge converter, and AC power having the same peak value as the amplitude of DC power is applied to the transformer, which has the advantage of the low turns ratio of the transformer. However, since the number of switching devices of the inverter for applying AC power is four, there is a disadvantage: the number of switching devices is more significant than that of other topologies [1], [55], [56], [57]. In addition, to form an AC magnetic flux in a transformer, two switches are always turned on, occurring conduction losses. In particular, the loss must be considered in inverters for low voltage and large currents such as fuel cells. Fig. 2(b) is a half-bridge converter, which has the advantage that the number of switching devices is half that of a full-bridge converter. There is a disadvantage in that the current flowing through the switching devices is doubled [58], [59], [60], [61]. Fig. 2(c) is a push-pull converter, and the voltage stress of the switching devices is mainly due to the leakage inductance of the transformer. There are disadvantages in that two sets of primary windings are required.

On the other hand, since the number of switching devices becomes half that of a full-bridge converter, the half-bridge reduces the total switching conduction loss, and the number of the turns ratio of the transformer is reduced. In a switching method for reducing switching loss, a push-pull converter is generally used, but the voltage stress of the switching devices is twice the input voltage. In particular, in a fuel cell system where the input voltage fluctuates, the transformer design of the push-pull converter is designed to be rated at the minimum input voltage. It must operate at the maximum input voltage. Therefore, the voltage stress of the switching devices has a disadvantage in that twice the maximum input voltage is applied [62], [63], [64], [65]. That is, it cannot be concluded that a specific method is superior, and a converter suitable for external conditions such as output voltage, current, and power of the fuel cell must be selected. Therefore, in this paper, by doubling the switching frequency of the buck converter, we propose a circuit structure that maximizes the advantages of the push-pull converter suitable for low-voltage, large-current applications through synchronizing control with the push-pull converter.

**B. CIRCUIT CONFIGURATION OF THE PROPOSED CONVERTER**

Fig. 3 shows the circuit configuration of the proposed dc-to-dc converter for the fuel cell. The power converter

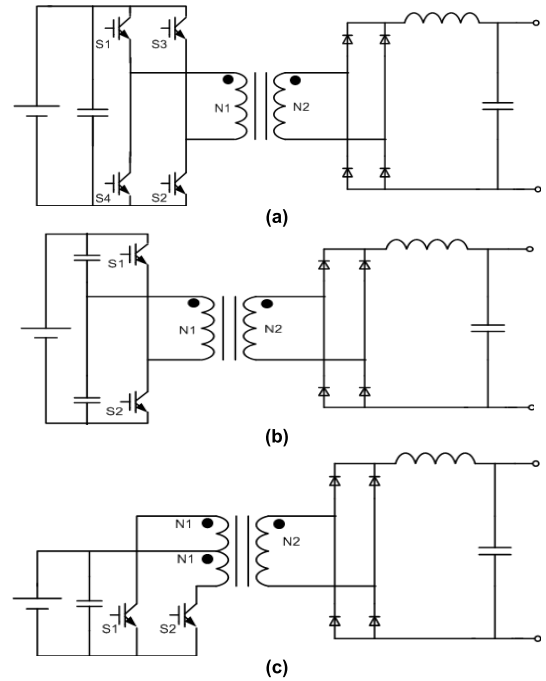


**FIGURE 2. Three representative circuit topologies used as fuel cell dc-to-dc converters. (a) Full-bridge converter, (b) Half-bridge converter, (c) Push-pull converter.**

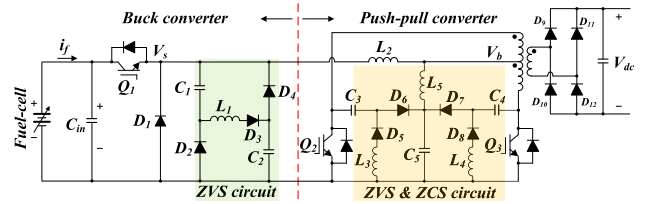


**FIGURE 3. Fuel-cell powered converter integrating buck converter and push-pull converter.**

comprises a buck converter for ZVS and a push-pull converter for ZVS and ZCS. The circuit structure is simple and economical if the converter is configured in a single-stage method. The two-stage way has disadvantages in that the number of switching elements and power loss increase, but it can cope with a wide range of input-output voltages [37], [38], [39], [40], [41], [42], [43]. The proposed converter has a structure in which the inductor of the non-isolated dc-to-dc converter and the current source inductor are shared. The circuit is composed of the same number of inductors as in the single-stage method, and the capacitor, the intermediate voltage source, is removed. In addition, it enables ZVS and ZCS by using the auxiliary circuit. In Fig. 3, the transformer is designed to make the rated output possible at the lowest value of the fluctuating input voltage. Therefore, the voltage applied to the switch at the lowest input voltage is the same between the conventional push-pull converter and the proposed converter. In a typical fuel cell system where the maximum input voltage is about 2.5 times the minimum input voltage, the voltage applied to the switching device becomes twice the maximum input voltage. However, as shown in Fig. 3, a push-pull converter

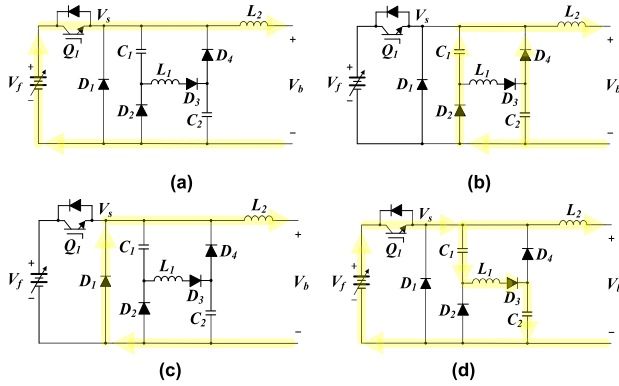


**FIGURE 4.** Operational mode of a buck converter with ZVS function, (a) mode A, (b) mode B, (c) mode C, (d) mode D.

combined with a buck converter is twice the minimum input voltage, so the voltage applied to the switch can be reduced by about 2.5 times. The conventional step-up push-pull converter forms a pulsed output current due to a low rate at a high input voltage. However, the converter in Fig. 3 can make a duty ratio of 0.5 to form a continuous output current regardless of the input voltage. In addition, the current peak of the push-pull converter can be reduced by operating the buck converter's switching frequency at twice the push-pull converter's switching frequency.

### C. OPERATIONAL MODE OF THE BUCK CONVERTER WITH AUXILIARY CIRCUIT

Fig. 4 shows the operational mode of a buck converter with the ZVS function. The inductor of the output stage of the buck converter is used as the inductor of the current source push-pull converter, so the capacitor for voltage smoothing has been removed. Mode A and C are the same as the operation mode of the existing buck converter, and the auxiliary circuit adds modes B and D for ZVS. When switched off by mode B, it becomes ZVS, and by mode D, the capacitor of the auxiliary circuit is charged in LC resonance mode [37].

Mode A starts when  $C_1$  and  $C_2$  are fully charged. If the current flowing through the inductor is  $I_{L_2}(0)$ , the current flowing through the switch  $Q_1$  is expressed as follows.

$$i_{Q_1}(t - t_1) = i_{L_2} = \frac{V_f - V_b}{L_2}(t - t_1) + I_{L_2}(t_0) \quad (1)$$

$$V_f = L_2 \frac{di_{L_2}(t - t_1)}{dt} + V_b \quad (2)$$

Mode B starts when switch  $Q_1$  turns off, and the energy stored in  $C_1$  and  $C_2$  is discharged through  $L_2$ . At this time, the current flowing through the diode and the capacitor voltage is expressed as follows.

$$i_{D_2}(t - t_2) = I_{L_2}(t_1) \cos \omega_2(t - t_2) - \frac{V_f}{Z_2} \sin \omega_2(t - t_2) \quad (3)$$

$$v_{C_1}(t - t_2) = I_{L_2}(t_1) Z_2 \sin \omega_2(t - t_2) + V_f \cos \omega_2(t - t_2) \quad (4)$$

where  $\omega_2 = \frac{1}{\sqrt{L_2 C_{12}}}$ ,  $Z_2 = \sqrt{\frac{L_2}{C_{12}}}$ ,  $C_{12} = C_1 + C_2$ .

Mode C starts when both  $C_1$  and  $C_2$  are discharged. The freewheeling by the diode  $D_1$  starts. At this time, the current flowing through the diode is as follows.

$$i_{D_1}(t - t_3) = i_{L_2} = \frac{-V_b}{L_2}(t - t_3) + I_{L_2}(t_2) \quad (5)$$

Mode D starts when switch  $Q_1$  is turned on. At this time, energy is charged to  $C_1$  and  $C_2$  through resonance with  $L_1$ , and ZVS becomes possible. The current flowing through the inductor and the capacitor voltage is expressed as

$$i_{L_1}(t - t_4) = \frac{V_f}{Z_4} \sin \omega_4(t - t_4) \quad (6)$$

$$v_{C_1}(t - t_4) = \frac{C_{12}}{C_1} [-V_f \cos \omega_4(t - t_4) + V_f] \quad (7)$$

$$v_{C_2}(t - t_4) = \frac{C_{12}}{C_2} [-V_f \cos \omega_4(t - t_4) + V_f] \quad (8)$$

where  $\omega_4 = \frac{1}{\sqrt{L_1 C_{12}}}$ ,  $Z_4 = \sqrt{\frac{L_1}{C_{12}}}$ ,  $C_{12} = \frac{C_1 C_2}{C_1 + C_2}$ .

### D. OPERATIONAL MODE OF THE PUSH-PULL CONVERTER WITH AUXILIARY CIRCUIT

In Fig. 3, the filter capacitor voltage  $v_{c_5}$  is determined by the voltage connecting the inductor  $L_5$ . Inductor  $L_5$  is connected to the neutral tap terminal of the push-pull converter in the front-end stage and is controlled by the buck converter as the minimum fuel cell voltage. Therefore,  $v_b$  is always a constant voltage, so the capacitor  $V_{C_5}$  can be considered a constant voltage source. The push-pull converter is described by dividing it into six operation modes.

Mode A [ $t_0 \sim t_1$ ]: It starts when  $Q_3$  is turned on when  $Q_2$  of the push-pull converter maintains on state and forms a current loop, as shown in Fig. 5(a). Both windings of the transformer's primary are short-circuited, and the secondary current of the push-pull converter becomes zero. In addition, the auxiliary circuit's capacitor voltage ( $v_{c_4}$ ), which was charged in positive polarity, forms a resonance circuit through the  $C_4$ - $Q_3$ - $L_4$ - $D_8$  loop. When the switch is turned off, the negative voltage is caused by the current as in (10) for ZVS.

$$i_{Q_2}(t - t_0) = \frac{V_s}{L_2 + L_{P_1}} + I(t_0) \quad (9)$$

$$i_{Q_3} = i_{L_{P_2}} + i_{C_4} = \frac{V_{C_4}(t_0)}{Z_0} \sin \omega_0 t + \frac{V_s}{L_2 + L_{P_2}} + I(t_0) \quad (10)$$

where  $Z_0 = \sqrt{\frac{L_4}{C_4}}$ ,  $\omega_0 = \frac{1}{\sqrt{L_4 C_4}}$ .

Suppose the inductance of the inductor of the output stage of the buck converter is sufficiently more prominent than the leakage inductance of the transformer. In that case, the current flowing through the inductor of the buck converter can be regarded as a constant current source. Therefore, since the primary current of the transformer flows by half of the inductance current of the buck converter, the switch transient loss is reduced when the switch is turned off. The leakage

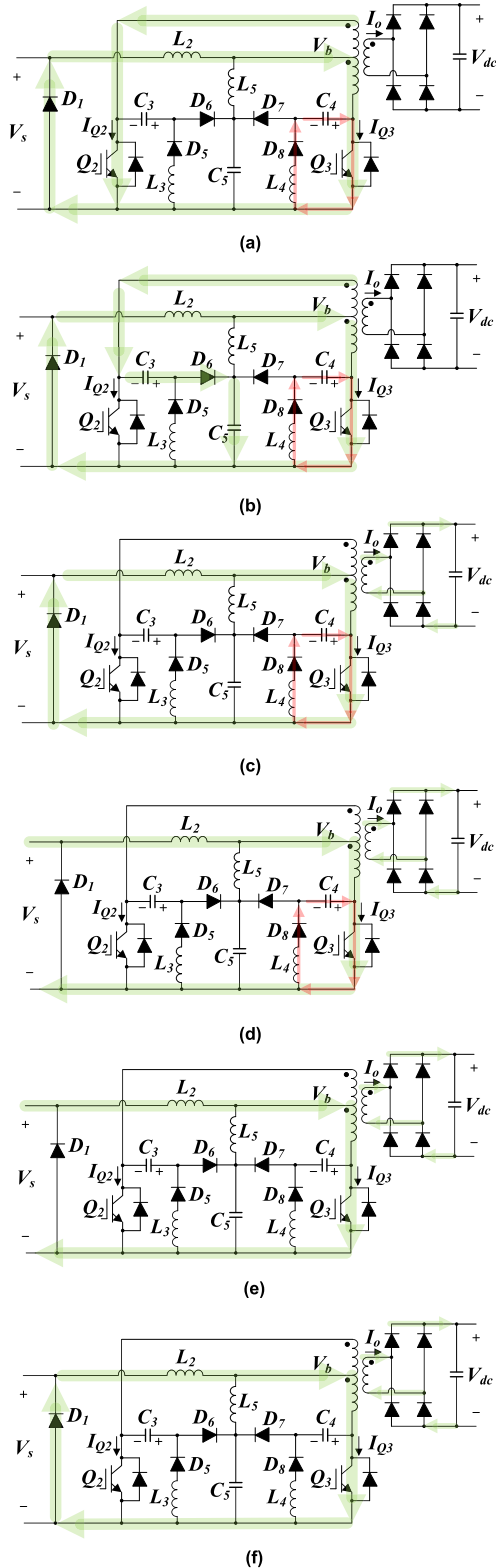


**FIGURE 5.** The operational mode of the push-pull converter with ZVS and ZCS function, (a) mode A, (b) mode B, (c) mode C, (d) mode D, (e) mode E, (f) mode F.

inductance determines the rate of increase of the switch current, and ZCS is formed when the leakage inductance of the transformer turns the switch on.

Mode B [ $t_1 \sim t_2$ ]: It starts when  $Q_2$  is turned off and forms a current loop, as shown in Fig. 5(b). When  $Q_2$  is turned off, the primary current of the transformer forms a current loop through  $C_3$ - $D_6$ - $C_5$ . As shown in (13), as the polarity of the capacitor voltage  $v_{C3}$  is changed by the  $i_{C3}$  current, the voltage applied to the switching device becomes zero, so ZVS is possible when the switch is off.

$$i_{Q3} = i_{L_{P2}} + i_{C4} = \frac{V_{C4}(t_1)}{Z_0} \sin \omega_0(t - t_2) + \frac{V_s}{L_2 + L_{P2}} + I(t_1) \quad (11)$$

where  $Z_0 = \sqrt{\frac{L_4}{C_4}}$ ,  $\omega_0 = \frac{1}{\sqrt{L_4 C_4}}$ .

$$i_{C3} = \frac{V_s}{Z_1} \sin \omega_1(t - t_2) + I(t_1) \quad (12)$$

$$v_{C3}(t - t_2) = \frac{C_{35}}{C_3} [-V_s \cos \omega_1(t - t_2) + V_s] \quad (13)$$

$$v_{C5}(t - t_2) = \frac{C_{35}}{C_5} [-V_s \cos \omega_1(t - t_2) + V_s] \quad (14)$$

where  $Z_1 = \sqrt{\frac{L_{2P1}}{C_{35}}}$ ,  $\omega_1 = \frac{1}{\sqrt{L_{2P1} C_{35}}}$ ,  $C_{35} = \frac{C_3 C_5}{C_3 + C_5}$ ,  $L_{2P1} = L_2 + L_{P1}$ .

Mode C [ $t_2 \sim t_3$ ]: It starts when the capacitor ( $C_3$ ) current becomes zero and forms a current loop, as shown in Fig. 5(c). At this time, current flows only in the lower winding of the transformer's primary. The primary energy is transferred to the secondary, and this mode occurs for a brief period.

$$i_o(t - t_3) = \frac{N_{12}}{N_2} \left[ \frac{V_{C4}(t_2)}{Z_3} \sin \omega_3(t - t_3) + \frac{V_s}{L_2 + L_{P2}} + I(t_2) \right] \quad (15)$$

where  $Z_3 = \sqrt{\frac{L_4}{C_4}}$ ,  $\omega_3 = \frac{1}{\sqrt{L_4 C_4}}$ .

Mode D [ $t_3 \sim t_4$ ]: It starts when the switch  $Q_1$  of the buck converter turns on, forming the current loop in Fig. 5(d). At this time, the input power is transferred to the output stage. The current slope flowing in the primary winding of the transformer is determined by the inductor  $L_2$  connected to the output side of the buck converter.

$$i_{Q3}(t - t_4) = \frac{V_{C4}(t_3)}{Z_0} \sin \omega_0(t - t_4) + \frac{V_s}{L_2 + L_{P2}} + I(t_3) \quad (16)$$

where  $Z_0 = \sqrt{\frac{L_4}{C_4}}$ ,  $\omega_0 = \frac{1}{\sqrt{L_4 C_4}}$ .

Mode E [ $t_4 \sim t_5$ ]: It starts when the resonance by the  $C_4$ - $Q_3$ - $L_4$ - $D_8$  loop is completed and forms a current loop, as shown in Fig. 5(e). If  $Q_3$  is turned off before this mode starts, ZVS will fail. Therefore, the starting point of this mode is a factor that determines the minimum duty ratio for ZVS.

$$i_{Q3}(t - t_5) = \frac{V_s}{L_2 + L_{P2}} + I(t_4) \quad (17)$$

$$i_o(t - t_5) = \frac{N_{12}}{N_2} \left[ \frac{V_s}{L_2 + L_{P2}} + I(t_4) \right] \quad (18)$$

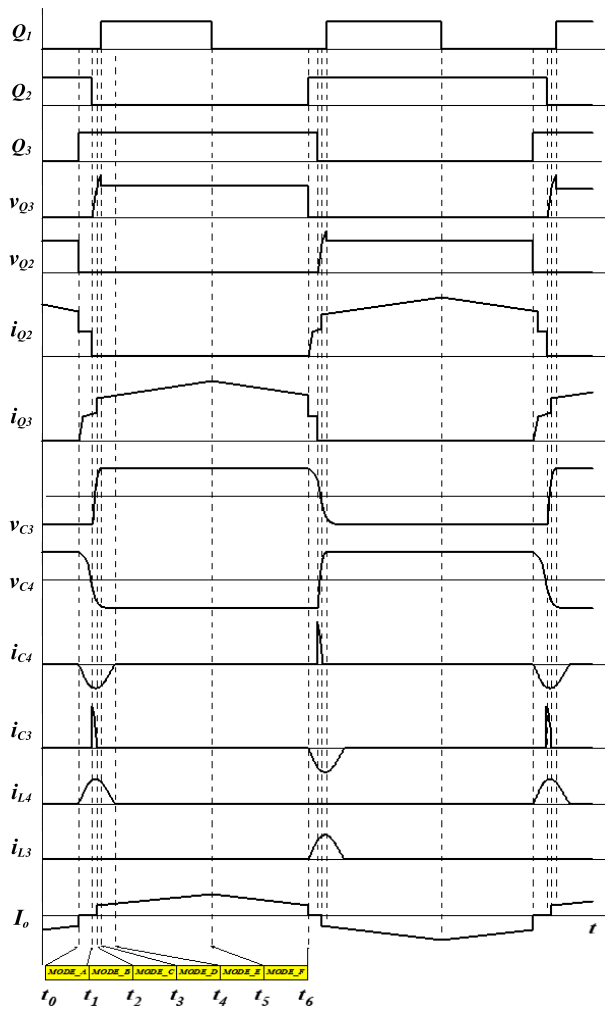


**FIGURE 6.** Fundamental waveforms of the fuel-cell-powered push-pull converter with ZVS and ZCS function.

Mode F [ $t_5 \sim t_6$ ]: It starts when  $Q_1$  of the buck converter is turned off and forms the current loop in Fig. 5(f). In this mode, the switching frequency of the buck converter is double that of the push-pull converter, and the switching between the two power converters is synchronized. Under this condition, the primary current ripple of the transformer is reduced by half, thereby reducing the power capacity of the transformer and the conduction loss of the switching device.

Fig. 6 shows the proposed converter's switching signal and critical operation waveform with the auxiliary circuit.

Fig. 7 compares the output current of the conventional push-pull converter with the output current of the proposed converter. In the conventional push-pull converter, if both push-pull converter switches are turned on simultaneously for step-up, the step-up inductor accumulates energy. Therefore, no current flows to the transformer's secondary, and the output current becomes discontinuous, as shown in Fig. 7(a). On the other hand, in the proposed converter, since the period where both push-pull converter switches are turned on simultaneously is very short, the transformer secondary

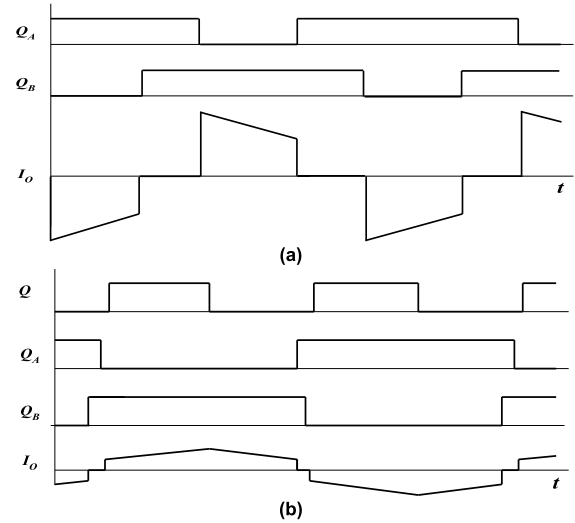


**FIGURE 7.** Comparison of output current between the existing push-pull converter and the proposed converter, (a) the existing push-pull converter, (b) the proposed push-pull converter.

current flows in the form shown in Fig. 7(b). When the output voltage and output power are constant, the peak current of the proposed converter is reduced compared to the output current of the conventional push-pull converter, and the value is determined by the inductor and duty ratio of the converter [37], [44], [45], [46], [47], [48], [49], [50].

### E. CONTROLLER DESIGN

Unlike general dc power, the output voltage of a fuel cell system has a drooping characteristic in which the output voltage decreases as the output current increases. Therefore, the controller for a fuel-cell-powered converter can have excellent operating characteristics only when a controller design is made considering the features of the fuel cell.

Fig. 8 shows the fuel cell equivalent circuit and the proposed converter.  $R_1$  and  $R_2$  are the fuel cell losses determined by fuel cell temperature and output current, and  $C_1$  is the capacitive component of the fuel cell stack. If the time constant of the converter controller is configured to be ten times larger than the time constant of the fuel cell, the time constant of the fuel cell can be ignored. In particular, in the case of grid-connected converters, since the difference in time constant is not an essential factor in the controller's configuration, the converter is designed on the assumption that the time constant of the controller is ten times greater than the time constant of the fuel cell.

If the duty ratio of the push-pull converter switch is kept constant at 0.5, it simply operates as a voltage amplifier. The buck converter switch controls the output voltage by the  $\delta(t)$  generated through PWM by the control signal  $v_c(t)$ . At this time, the output voltage of the converter is determined by the duty ratio ( $d$ ), the input voltage ( $V_g(t)$ ), and the output current ( $i_{load}(t)$ ). The controller can control the duty ratio, but the controller cannot govern the input and output voltage.

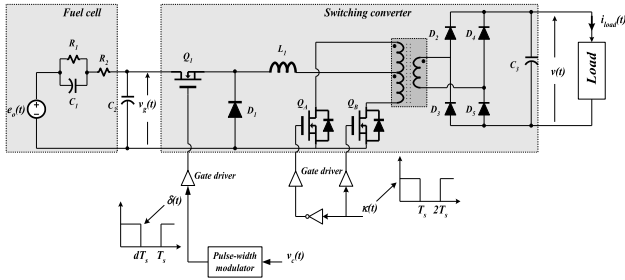


FIGURE 8. Fuel cell equivalent circuit and proposed converter configuration.

Therefore, input and output voltage are disturbances when designing the controller.

Fig. 9 shows the conceptual control diagram of the fuel-cell-powered converter. The converter’s output  $V(t)$  is determined by the duty ratio, input voltage, and output current. However, the factor that can control the output is only the duty ratio. Therefore, it should be possible to obtain desired control characteristics through duty ratio controller design. The output voltage for applying the small-signal model in the converter system in Fig. 9 follows.

$$v(s) = V + \hat{v}(s)$$

$$d(s) = D + \hat{d}(s)$$

$$i_{load}(s) = I_{load} + \hat{i}_{load}(s) \tag{19}$$

$$\hat{v}(s) = G_{vd}(s)\hat{d}(s) + G_{vg}(s)\hat{v}_g(s) - Z_{out}(s)\hat{i}_{load}(s) \tag{20}$$

$$G_{vd}(s) = \left. \frac{\hat{v}(s)}{\hat{d}(s)} \right|_{\hat{v}_g = 0, \hat{i}_{load} = 0}$$

$$G_{vg}(s) = \left. \frac{\hat{v}(s)}{\hat{v}_g(s)} \right|_{\hat{d} = 0, \hat{i}_{load} = 0}$$

$$Z_{out}(s) = \left. \frac{\hat{v}(s)}{\hat{i}_{load}(s)} \right|_{\hat{d} = 0, \hat{v}_g = 0} \tag{21}$$

Fig. 10 shows a small-signal block diagram of a fuel-cell-powered converter. Since the value of gain error or disturbance cannot be known in advance, it cannot be reflected when determining the gain of the open-loop controller. With the structure of the open-loop controller, there is no way to eliminate or reduce the gain error or output error due to disturbance. As shown in Fig. 10, the output voltage error according to the input voltage change is determined by the  $G_{vg}(s)$  transfer function.

Moreover,  $G_{vg}(s)$  cannot be compensated by the output voltage control factor, and the power circuit must be configured to minimize  $G_{vg}(s)$ . Also, the output current fluctuation has the same characteristics as the input voltage fluctuation. To improve this problem, feedback control is generally used, and the composition of the duty ratio controller to control the

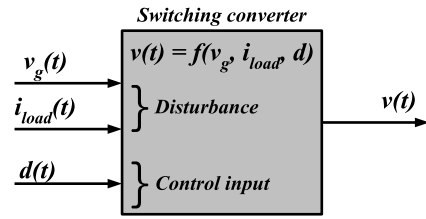


FIGURE 9. Control concept diagram for the fuel-cell-powered converter.

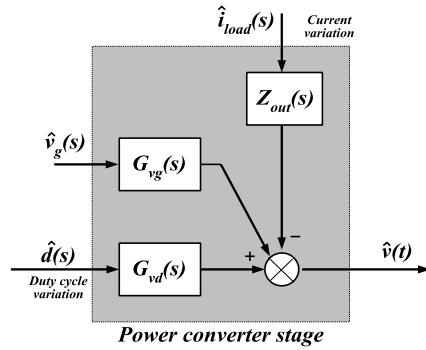


FIGURE 10. Small signal block diagram of the fuel-cell-powered converter.

output voltage is shown in Fig. 11. The purpose of the feedback controller is to maintain a constant output voltage even when the input voltage or load current changes. However, the duty ratio is impossible to obtain a constant output voltage for all conditions with one control variable. Therefore, it is necessary to design the power circuit and the controller according to the fluctuation range of the input voltage. The output voltage of the converter operates as a compensator. It controls the switching signal of the buck converter using the error signal  $v_e$ , which is the difference between the output voltage detection signal  $S_V$  through the voltage sensor and the filter circuit and the output voltage command value. At this time, the compensator’s design determines the dc-to-dc converter’s operating characteristics.

Fig. 12 shows a voltage control block diagram of fuel-cell-powered converters. The small-signal model of the converter and the voltage regulator shown in Fig. 10 are needed to analyze the output voltage feedback control operation.

From Fig. 13, the output voltage variation is as follows.

$$\begin{aligned} \hat{v}(s) = & \frac{G_c(s)G_{vd}(s)/V_M}{1 + S(s)G_c(s)G_{vd}(s)/V_M} \hat{v}_{ref}(s) \\ & + \frac{G_{vg}(s)}{1 + S(s)G_c(s)G_{vd}(s)/V_M} \hat{v}_g(s) \\ & - \frac{Z_{out}(s)}{1 + S(s)G_c(s)G_{vd}(s)/V_M} \hat{i}_{load}(s) \end{aligned} \tag{22}$$

If (22) is rearranged using the loop gain  $T(s)$ ,

$$\hat{v}(s) = \frac{1}{S(s)} \frac{T(s)}{1 + T(s)} \hat{v}_{ref}(s)$$

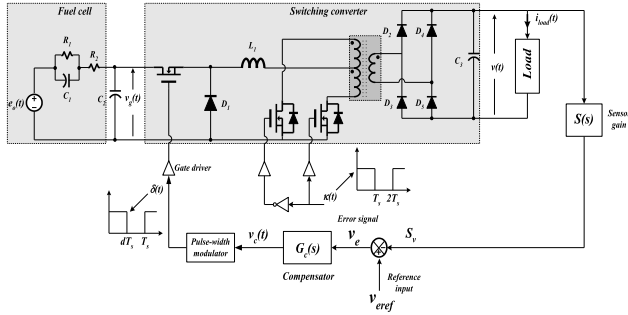


FIGURE 11. Voltage control of fuel-cell-powered converters.

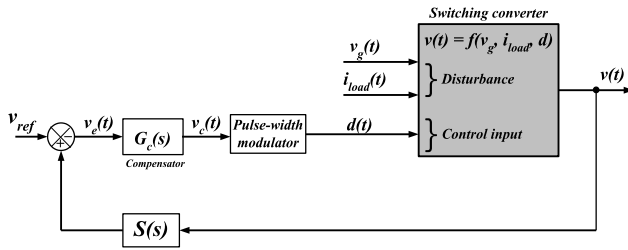


FIGURE 12. Voltage control block diagram of fuel-cell-powered converters.

$$\begin{aligned}
 & + \frac{G_{vg}(s)}{1 + T(s)} \hat{v}_g(s) \\
 & - \frac{Z_{out}(s)}{1 + T(s)} \hat{i}_{load}(s)
 \end{aligned} \quad (23)$$

The loop gain  $T(s)$  is defined by

$$T(s) = \frac{S(s)G_c(s)G_{vd}(s)}{V_M} \quad (24)$$

According to the high gain theorem, the larger the loop gain  $T(s)$ , the less the influence of disturbance and the better the command follows. It is effective when the control target is command-following and there is no measurement noise in the target system. If the loop gain is considerable and the following condition is satisfied, (23) can be expressed as (25).

$$\hat{v}(s) = \frac{1}{S(s)} v_{ref}(s) \quad @ |T(s) \gg 1| \quad (25)$$

As seen in (25), the output is determined by the transfer function of the measuring sensor. Therefore, an output voltage error will naturally occur if a disturbance occurs in the transfer function  $S(s)$  of the measuring sensor and the filter circuit. After all, since the accuracy of the sensor and filter circuit is critical, the filter part is digitized in this paper so that it is not affected by temperature or other surrounding factors. (25) equally applies to the steady-state and is the same as (26).

$$\frac{V}{V_{ref}} = \frac{1}{S(0)} \frac{T(0)}{1 + T(0)} \approx \frac{1}{S(0)} \quad (26)$$

For the output voltage to follow the reference voltage,  $S(0)$  must be accurately set, and the loop gain  $T(0)$  must be significant. The sensor of  $S(s)$  must be precise, and the precision of the PWM power stage, which is the compensator gain, may

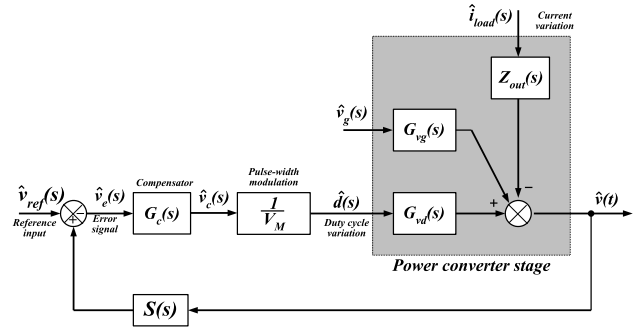


FIGURE 13. Overall small-signal block diagram of the fuel-cell-powered converter.

be small. By performing the feedback control in this way, the sensitivity to the forward path gain is reduced, and at the same time, the sensitivity to the feedback path gain is increased. The stability of the system can be determined directly by the magnitude and phase of  $T(s)$ . That is, to obtain good performance in a transfer function including  $1/(1+T(s))$ , the shape of  $T(s)$  must be determined. The corner frequency ( $f_c$ ) of  $T(s)$  can be obtained by (27).

$$\|T(j2\pi f_c)\| = 1 \quad (27)$$

The phase margin  $\varphi_m$  is the value obtained by adding 180 to the phase at the corner frequency.

$$\Phi_m = 180^\circ + \angle T(j2\pi f_c) \quad (28)$$

The necessary and sufficient conditions for the system's stable operation are that the corner frequency is one and the positive phase margin.

#### F. BATTERY CHARGING METHOD USING OXYGEN AMOUNT CONTROL

A fuel cell generally uses a battery or an ac-to-dc converter for initial start-up. However, replacing the battery periodically or configuring a separate charger is necessary. This paper proposes a new method for charging a battery by controlling the amount of oxygen in the fuel cell system without using a charger. This method is considered to have significant advantages in performance and efficiency improvement when used for battery charging by using the inherent characteristics of low voltage and high current, which are the characteristics of fuel cells. Since the fuel cell stack uses hydrogen gas and oxygen as fuel, the activity increases in proportion to the partial pressure. The electromotive force (emf) also increases proportionally to the hydrogen gas and oxygen pressure. To construct a direct fuel cell charger without a power converter using these characteristics, the relationship between the electromotive force according to hydrogen gas and oxygen pressure is as follows.

$$E = E^o + \frac{RT}{2F} \left[ \ln P_{H_2} + \ln P_{O_2}^{\frac{1}{2}} - \ln P_{H_2O} \right] \quad (29)$$



$E^o$  is the standard emf (Electromotive force).  $P_{H2}$  is the emf change term according to the pressure of hydrogen gas.  $P_{O2}$  is the emf term that changes according to oxygen gas pressure.

Since the back electromotive force is proportional to the pressures of hydrogen gas and oxygen, the power generation voltage of the fuel cell can be controlled by controlling the hydrogen gas or oxygen pressure. In general, the pressure of hydrogen gas in the fuel cell system is fixed at 5bar, but the oxygen pressure has a structure that can be varied according to the amount of surrounding oxygen. Therefore, a method of controlling the fuel cell voltage by controlling the pressure of oxygen is adopted in this paper.

Fig. 14 shows the configuration diagram of the proposed direct charging method for fuel cells and a flowchart for the battery charging operation. At the initial start-up of the fuel cell, power is supplied from the battery to start the fuel cell. When the fuel cell output power is greater than the self-consumption power, the battery is removed, and the power obtained from the dc-to-dc converter using the self-generated power is used. The proposed fuel cell direct charging mode starts, and the charging switch SW2 is turned on to charge the battery with power generated from the fuel cell. The battery used in this study is a 12V lead-acid battery. The charging pattern of the constant current mode or constant voltage mode is determined by detecting the battery's state of charge from the current and voltage flowing through the battery at the initial charging stage. In Fig. 14(a), the Air Compressor is controlled through the proportional-integral controller based on the difference between the charging current command value and the actual charging current. Moreover, the fully charged voltage is determined by detecting the battery temperature based on the lead-acid battery's temperature characteristic table. When the battery voltage matches the charge completion voltage command value, the control right of the Air Compressor is transferred to the stack control unit to generate the output voltage in normal mode, and the output relay is turned on to create external power.

Fig. 15 shows the transient response characteristics when the load of the fuel cell stack is varied. The load current increases instantaneously, and the terminal voltage decreases accordingly. The air compressor determines the chemical reaction between hydrogen and oxygen. Still, it takes about 500ms for the output voltage to normalize because the response characteristic of the compressor is slow. Therefore, the power generation time constant of the fuel cell stack is about 500ms. If the time constant of the power converter using this is 10% or less compared to the time constant of the stack, the time constant of the power converter can be ignored. Therefore, the time constant of the power converter used in this paper is designed to be less than 50ms.

III. SIMULATION AND EXPERIMENTAL RESULTS

Fig. 16 shows the configuration for fuel cell connection using the proposed converter system. The TMS302F2812 controls the dc-to-dc converter and grid-connected inverter.

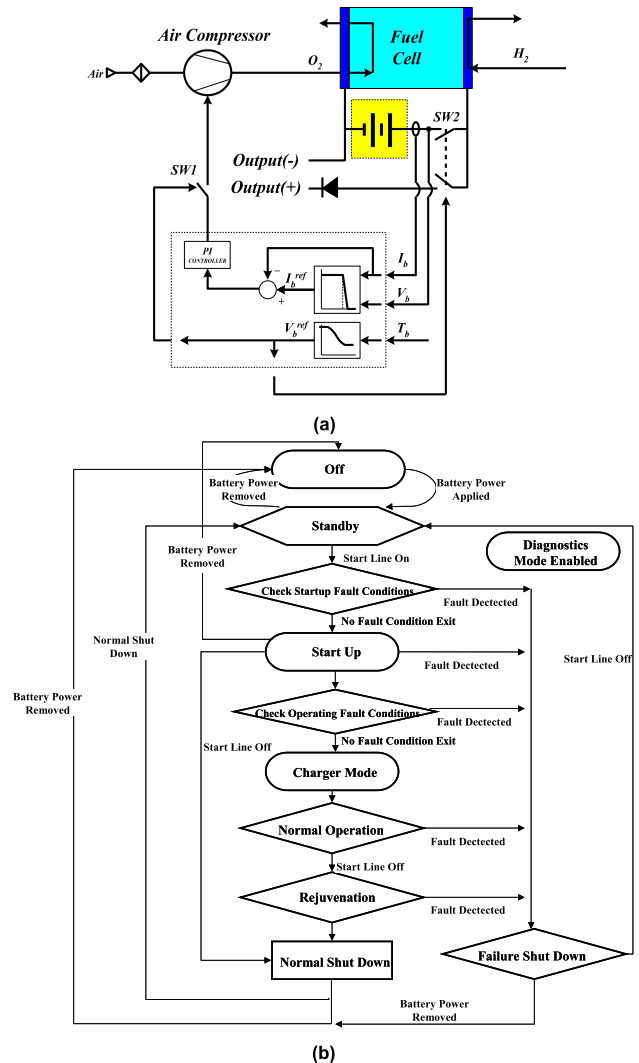


FIGURE 14. Structure and operation flow chart of the proposed direct charging method for fuel cell, (a) Direct charging method structure, (b) Battery charging operation flowchart.

A microprocessor is used to configure the host controller to control the state of the fuel cell and the output of the power conversion system. Based on the generated power of the fuel cell and the state of the fuel cell measured by the oxygen sensor and the temperature sensor, the actual fuel cell output characteristics and the output during the operation were taken into consideration. The amount of power that could be generated efficiently was controlled to be connected to the grid. In a fuel cell system, a new method of directly charging a battery in a fuel cell is applied by using the correlation characteristics between the amount of oxygen and the fuel cell voltage. By introducing a buck converter instead of a boost converter, it is possible to design a current source by not using a capacitor at the output stage of the converter. The grid-connected inverter includes over-voltage protection, over-current protection, protection according to frequency fluctuations, and islanding operation prevention functions that a grid-connected inverter must have [10], [51], [2], [3], [52], [53], [54].

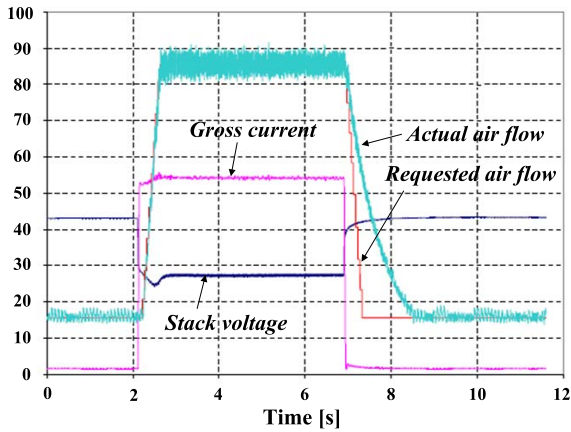


FIGURE 15. Transient response characteristics of fuel cell stack according to output.

Fig. 17 is a simulated waveform showing ZVS when buck converter  $Q_1$  is turned off. These are the switching signal,  $Q_1$  voltage,  $Q_1$  current,  $L_2$  current,  $C_1$  current,  $C_1$  voltage, and  $L_1$  current from top to bottom. When  $Q_1$  is turned off, the voltage applied to the switching device has a rise time of about  $1\mu s$ . When the  $Q_1$  switch is turned off, the output current of the buck converter shares the output current with the energy charged in the auxiliary circuit's two capacitors ( $C_1$  and  $C_2$ ), so ZVS of the  $Q_1$  switch is possible. The auxiliary circuit capacitors ( $C_1$  and  $C_2$ ) charge starts with the LC resonance when the switching device is turned on.

Fig. 18(a) is a simulation waveform for voltage and current of the proposed push-pull converter switch. ZVS is enabled when the switch is turned off, and ZCS is enabled when the switch is turned on. When the switch is turned off, the switch voltage doubles overshoot; to reduce this voltage, the capacitor capacity of the auxiliary circuit can be increased to minimize it. Still, reactive power by the push-pull converter is increased. Fig. 18(b) shows the capacitor and inverter current and voltage of the auxiliary circuit of the push-pull converter. Fig. 18(c) shows the push-pull converter's regenerative power and output waveform. Since the  $C_5$  capacitor voltage and  $L_5$  inductor current are kept constant, the output voltage appears as good dc.

Fig. 19(a) shows the inverter's output voltage, grid current, and grid voltage when the fuel cell system is connected to the grid voltage, including the 3<sup>rd</sup> and 5<sup>th</sup> harmonics. The grid current also contains many harmonics as harmonic components of the grid voltage. If the inverter operates under the condition that the grid voltage is sinusoidal, the harmonic component of the grid current cannot be removed. To solve this, there is a way to increase the size of the inductor, but the weight and cost increase. Fig. 19(b) shows the inverter output voltage, grid current, and grid voltage when the harmonic component of grid voltage is compensated. It was confirmed that a good grid current could be obtained by compensating the harmonic component of the output voltage obtained through FFT with the feedforward term.

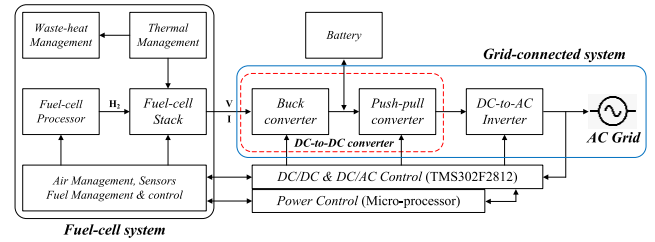


FIGURE 16. System configuration for grid connection of fuel cells using the proposed converter.

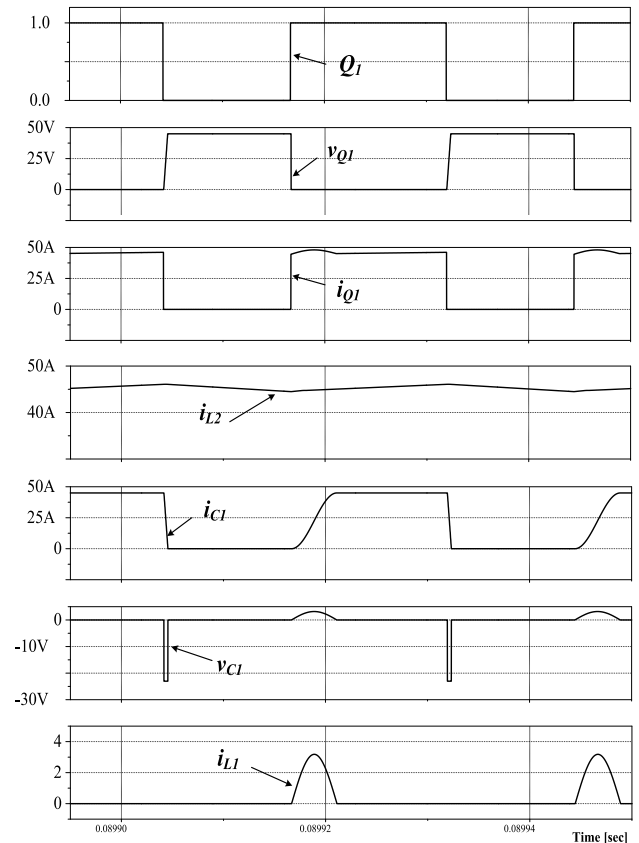
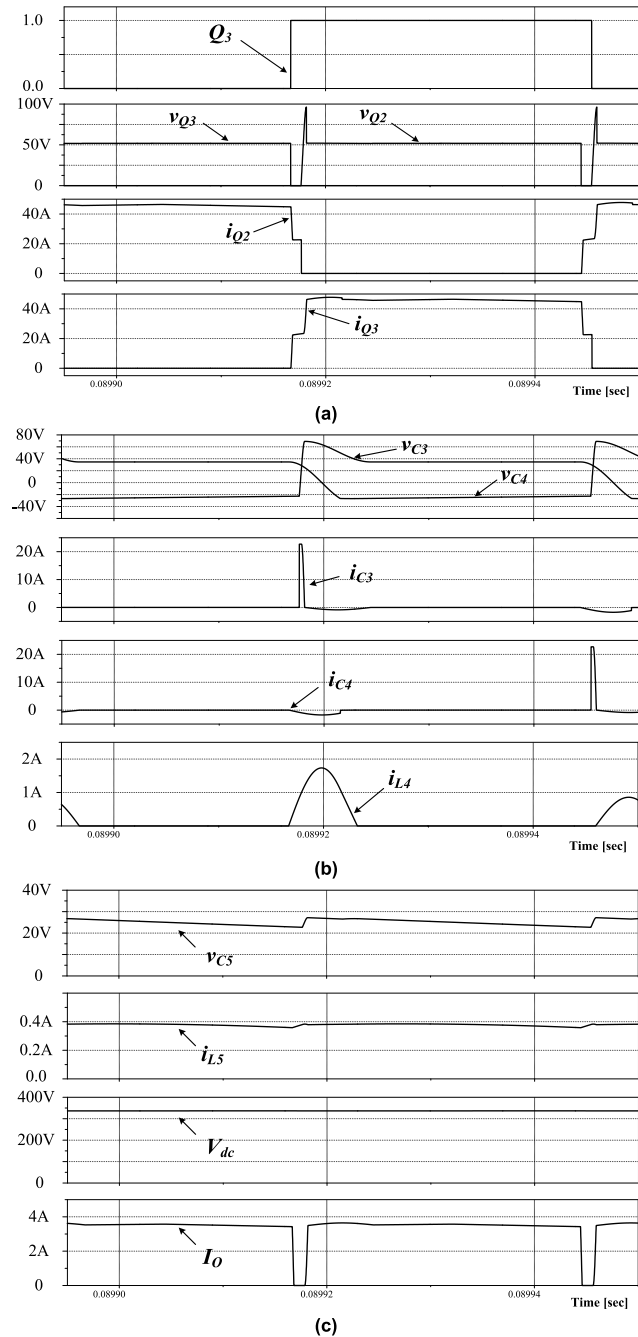


FIGURE 17. Fundamental operating waveforms of buck converter stage, switching signal,  $Q_1$  voltage,  $Q_1$  current,  $L_2$  current,  $C_1$  current,  $C_1$  voltage, and  $L_1$  current from top to bottom.

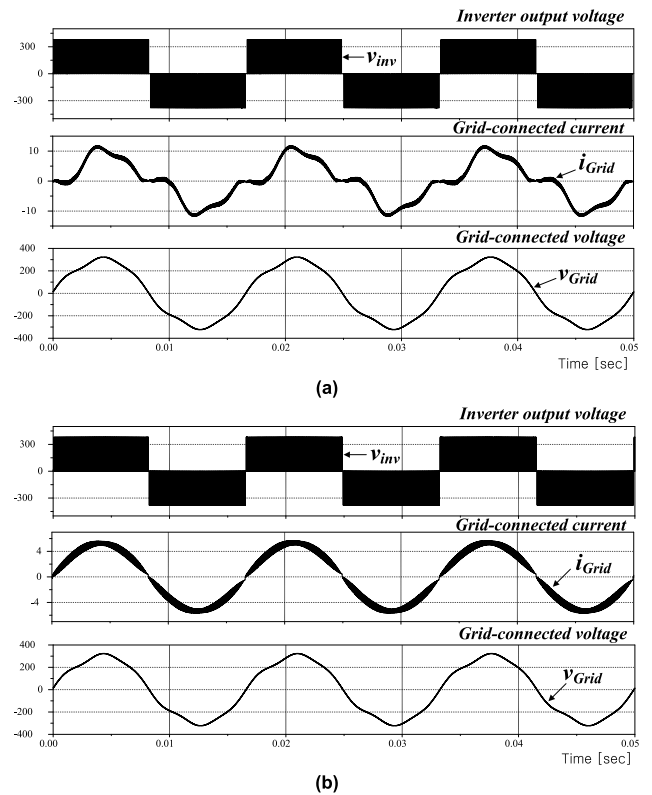
Fig. 20 shows a prototype of the proposed converter for the fuel cell. The controller is designed based on TMS302F2812. Detailed specifications are shown in Table 1. It is designed with a power capacity of 1kW, and the operating voltage of the fuel cell is 66~150V. The buck converter operates at 36kHz, and the push-pull converter operates at 18kHz switching frequency.

Fig. 21(a) shows the drain-source voltage, drain current, switching loss of the buck converter switch  $Q_1$ , and the inductor current of the auxiliary circuit. Fig. 21(b) is an enlarged waveform of Fig. 21(a) to confirm ZVS operation. It can be seen that the switching loss does not occur when off because the switch voltage rises after the switching current becomes zero.



**FIGURE 18.** Fundamental operating waveforms of the push-pull converter, (a) switch voltage and switch current, (b) capacitor voltage, capacitor current, inductor current in ZVS circuit, (c) Capacitor  $C_5$  voltage, inductor  $L_5$  current, output voltage, and output current.

Fig. 22 shows the primary waveforms of the push-pull converter. Fig. 22(a) shows the voltage across the push-pull converter switch  $Q_2$ , the switching power loss, the  $Q_2$  switch current, and the current flowing through the capacitor  $C_3$  of the auxiliary circuit. Fig. 22(b) is an enlarged waveform of the turn-on part of switch  $Q_2$  in Fig. 22(a) to check whether the ZCS operates. It shows the ZCS operation in which the current starts flowing after the voltage across the  $Q_2$  switch becomes zero. It can be seen that there is no switching loss



**FIGURE 19.** When connected to the grid containing 5% of the 3<sup>rd</sup> and 5<sup>th</sup> harmonics, the inverter output voltage, grid-connected current, grid voltage, (a) before harmonic component compensation, (b) harmonic component in the inverter voltage command is compensated with a feedforward term.

caused by the product of the voltage across the switch and the switch current. Fig. 22(c) is an enlarged waveform of the turn-off part of the switch in Fig. 22(a) to check whether ZVS operates. It shows that the voltage across the switch starts to rise after the switch current becomes almost zero.

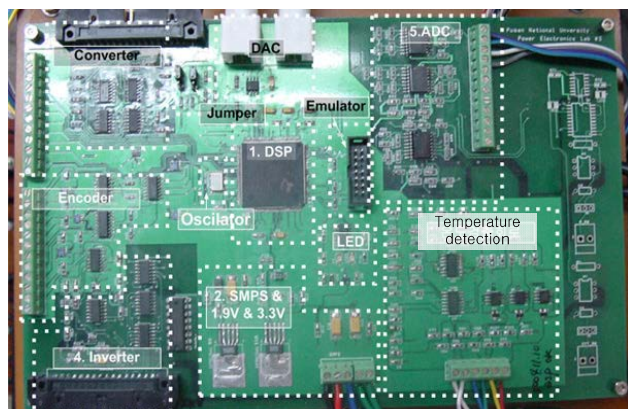
Fig. 23 shows the voltage and current ripple for each power conversion stage according to the ripple control method. Current ripple control can reduce the voltage ripple of the dc-link capacitor on the transformer’s secondary but has a problem of increasing the current ripple on the fuel cell side. On the other hand, in the voltage ripple control, the current ripple on the fuel cell can be reduced, but there is a problem that the voltage ripple of the dc-link capacitor increases. In this paper, voltage ripple control is applied to control the current ripple to 5% or less because it is more important to reduce the current ripple on the fuel cell to ensure the lifespan of the fuel cell. For the grid connection, the inverter needs a current controller, and the converter in the front stage needs a voltage controller, including a current controller. Since the DC current of a single-phase inverter is in the form of an absolute sine wave, the voltage ripple of the dc-link stage is considerable. Therefore, there is a problem that the lifecycle of the capacitor is shortened. To solve this, a method of compensating with the converter current in the front stage can be applied, but a problem arises that the converter current

**TABLE 1.** Specification of the proposed fuel-cell-powered converter.

Description	Value	Unit
Rated power	1.0	kW
Operating voltage range of fuel-cell	66~150	V
Power MOSFET - IRFP90N20D	200	V
	94	A
Diode - APT100S20B	200	V
	120	A
Switching frequency – Buck converter	36	kHz
Switching frequency – Push-pull converter	18	kHz
Inductor for Buck converter ( $L_2$ )	200	$\mu$ H
ZVS inductor for Buck converter ( $L_1$ )	20	$\mu$ H
ZVS capacitor for Buck converter ( $C_1, C_2$ )	15	nF
ZVS inductor for Push-pull converter ( $L_3, L_4$ )	40	$\mu$ H
ZVS capacitor for Push-pull converter ( $C_3, C_4$ )	22	nF
Turn-ratio of the transformer	1:6	Turns



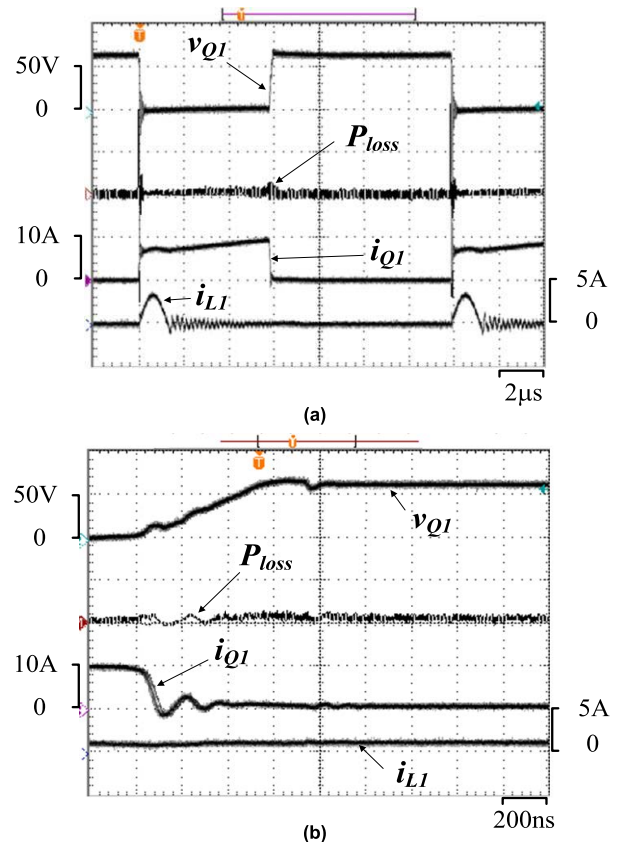
(a)



(b)

**FIGURE 20.** Photograph of 1kW prototype, (a) proposed fuel-cell-powered converter, (b) controller using TMS320F2812.

ripple becomes large. In this paper, the lifespan of the fuel cell is considered more important than the dc-link capacitor. Therefore, the voltage ripple of the dc-link stage is tolerated.

**FIGURE 21.** The experimental waveform of buck converter, (a) Drain-source voltage of  $Q_1$  switch, switching loss,  $Q_1$  switch current, auxiliary circuit  $L_1$  inductor current, (b) Time-division enlargement of (a).

It is possible to reduce the converter current ripple by changing the control gain of the converter. Setting the controller gain value according to the fuel cell input current ripple is necessary.

Table 2 shows the voltage and current gain values of Fig. 24. In a state where  $K_i$  of voltage gain and  $K_p$  of current gain are the same, if  $K_p$  of voltage gain and  $K_p$  of current gain are adjusted, ripple current can be controlled.

Table 3 compares the characteristics of three typical converter circuits for fuel cells and the proposed converter. Compare the voltage and current stress on the primary switch of the transformer, the fuel cell input current ripple, the transformer window utilization, the equivalent switching frequency, and angular frequency ( $\omega$ ) that changes the size of the inductor and capacitor.

Table 3 shows that the proposed converter's switch voltage and current stress are the same as those of the full-bridge and push-pull converter switches. However, the transformer of the proposed converter is designed so that the rated output is possible at the lowest value of the fluctuating fuel cell input voltage. A typical fuel cell system's maximum voltage is about 2.5 times the minimum. Therefore, in a general push-pull circuit structure, the voltage applied to the switch is twice the maximum input voltage. However, in the proposed design, a buck converter and a push-pull converter are combined to

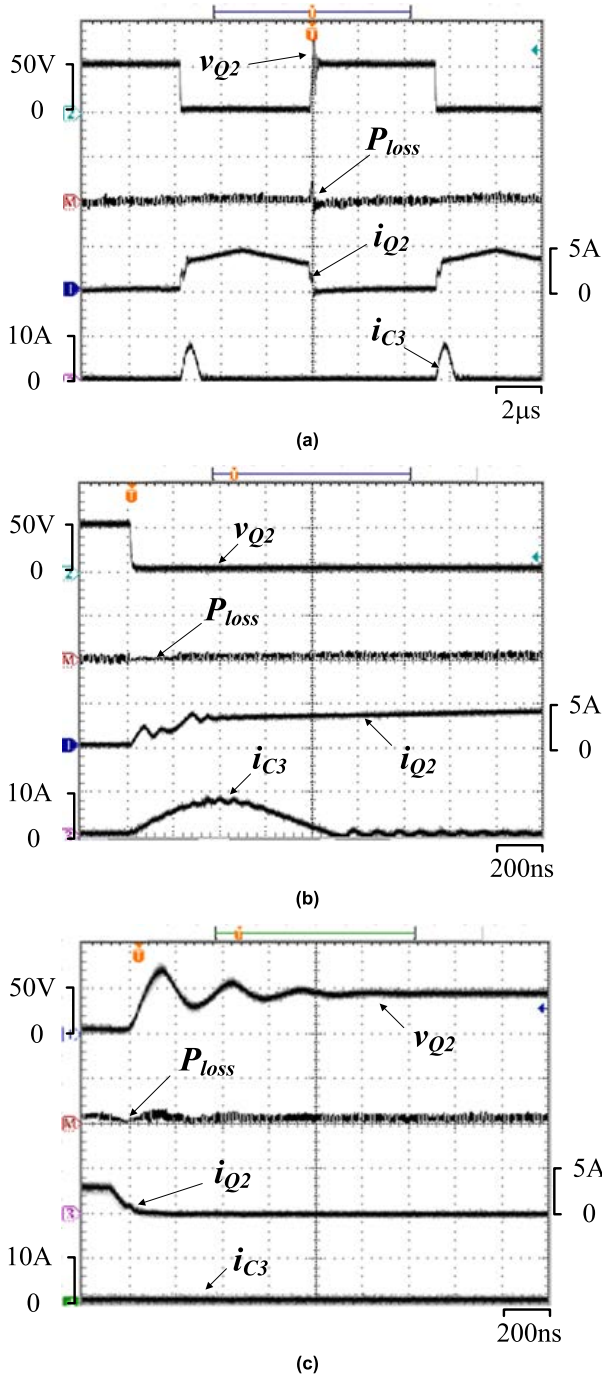


**FIGURE 22.** The experimental waveform of the push-pull converter, (a) Voltage across  $Q_2$  switch, switching loss,  $Q_2$  switch current, auxiliary circuit  $C_3$  capacitor current, (b) ZCS operation when turning on  $Q_2$ . (c) ZVS operation when turning off  $Q_2$ .

respond to a wide voltage range up to twice the minimum input voltage, so the voltage applied to the switch can be reduced by about 2.5 times. In addition, the current peak of the push-pull converter can be reduced because the switching frequency of the buck converter in the front stage is operated at twice the switching frequency of the push-pull converter in the rear stage.

**TABLE 2.** Voltage and current gains according to the ripple control method.

Control method	Voltage gain		Current gain	
	Ki	Kp	Ki	Kp
Current ripple control	50.0	2.1	1.0	0.1/20.
Voltage ripple control	50.0	0.1	10.0	0.1/20.

**TABLE 3.** Comparison of characteristics between the proposed converter and the existing three representative circuit methods.

	Half-bridge	Full-bridge	Push-pull	Proposed
Voltage stress @primary switch	$\frac{V_{in}}{(1-D)}$	$\frac{V_{in}}{2(1-D)}$	$\frac{V_{in}}{2(1-D)}$	$\frac{V_{in}}{2(1-D)}$
Current stress @primary switch	$2I_{in}$	$I_{in}$	$I_{in}$	$I_{in}$
Input current ripple	Moderate	Moderate	Moderate	Good
Transformer windows utilization	Good	Good	Poor	Good
Equivalent switching frequency @secondary	$2f_s$	$2f_s$	$2f_s$	$4f_s$
Angular frequency, $\omega$	$4\pi f_s$	$4\pi f_s$	$4\pi f_s$	$8\pi f_s$

The selection of the DC smoothing capacitor’s capacitance is vital in determining the system time constant that determines the characteristics of the converter and reducing the ripple of the DC voltage.

In Fig. 25,  $i_{dc-out}$  is the current flowing from the DC power source to the grid through the inverter, and  $i_{dc-in}$  is the current flowing into the capacitor from the dc-to-dc converter. Therefore, the integral difference between the two currents generates the DC voltage ripple. As given in (30), the grid voltage ( $v_{Grid}$ ) and the inverter rating ( $P_{inv}$ ) determine the current ( $i_{inv}$ ) flowing into the power source.

$$i_{inv} = \frac{P_{inv}}{v_{Grid}} \tag{30}$$

At this time, the current flowing into the capacitor is determined by the current flowing into the grid. In Fig. 25, area A and area B become the same operating parallel point, and the value is the same as (31).

$$i_{dc-in} = \frac{2\sqrt{2}}{\pi} I_{inv} \tag{31}$$

As shown in Fig. 25, the current flowing into the capacitor is a constant DC current, but the current flowing into the grid has a pulsating component.  $\Delta Q$ , the integral difference between the two currents generated by the pulsation, can be obtained by (32).

$$\Delta Q = \int_{\theta_1}^{\theta_2} \left[ I_{max} \sin(2\pi t) - \frac{2}{\pi} I_{max} \right] \cdot dt \tag{32}$$

The voltage fluctuation of the capacitor due to  $\Delta Q$  obtained in (32) is as shown in (33).

$$\Delta V = \frac{\Delta Q}{C_{dc}} \tag{33}$$

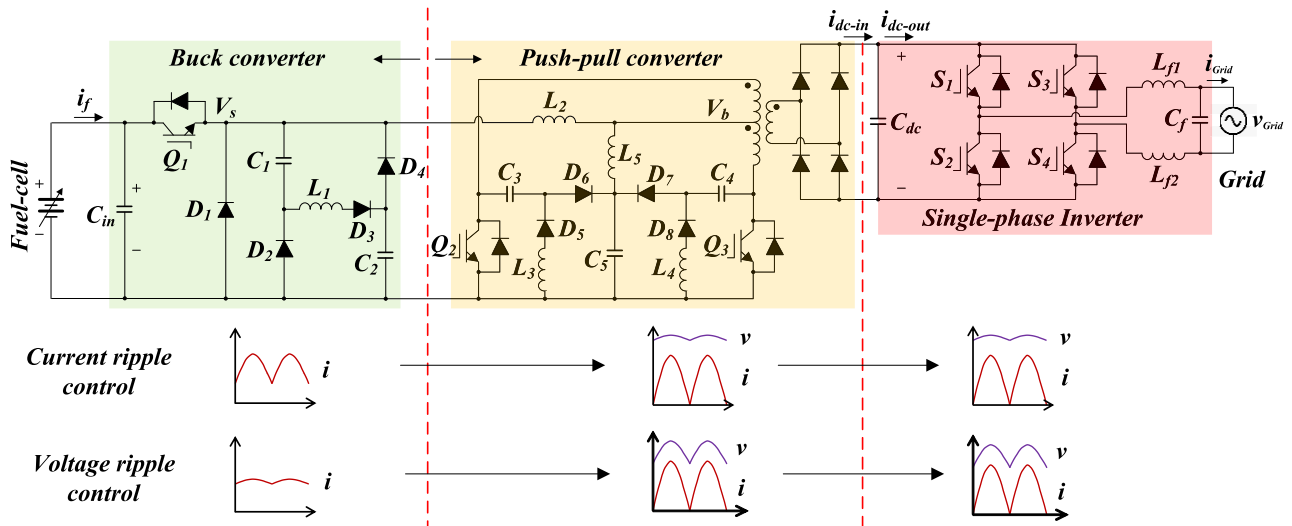


FIGURE 23. Voltage and current ripple for each power conversion stage according to the ripple control method.

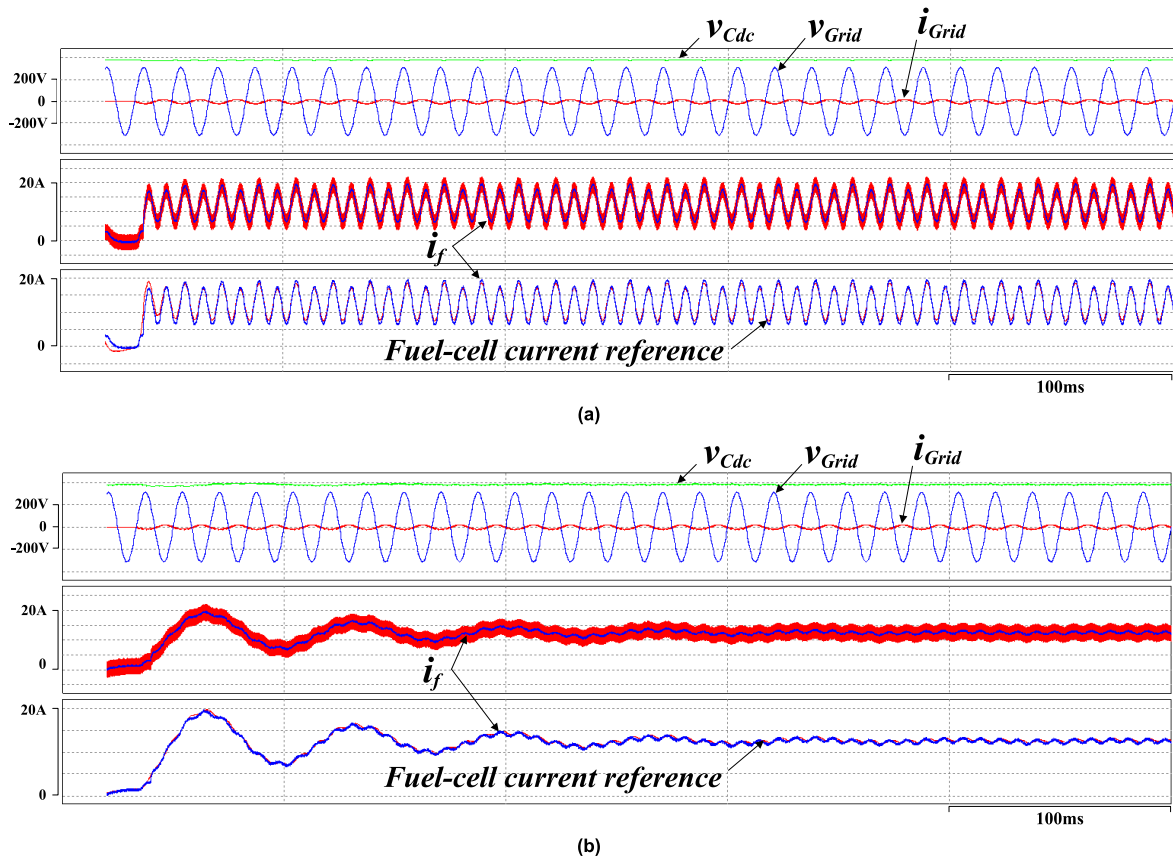
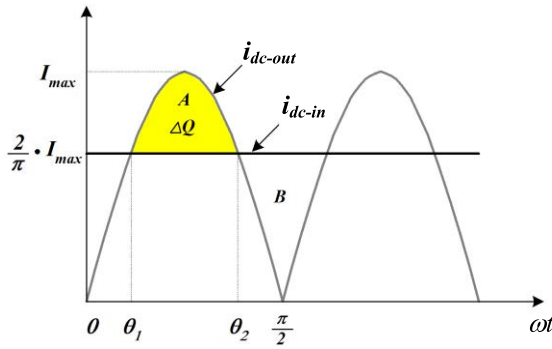


FIGURE 24. Fuel cell output current, DC-link voltage, grid voltage, and grid current according to the ripple control method, (a) current ripple controller, (b) voltage ripple controller.

If the ripple rate of the DC voltage is set to 5% or less, the capacitance of the capacitor may be set to a value that satisfies the conditional (34).

$$C_{dc} = \frac{\Delta Q}{0.05V_{dc}} \quad (34)$$

The capacitance between the fuel cell and the Buck converter can also be calculated using (34). In the case of the input side, line inductance exists due to the distance between the fuel cell and the buck converter, and the ripple of the fuel cell current is controlled by voltage ripple control. In this paper, a capacitance of  $480\mu\text{F}$  is used.



**FIGURE 25.** Calculation of capacitance for DC power smoothing of the 1-grid-connected inverter.

Fig. 26(a) shows the inverter voltage, inverter current, and fuel cell output current under the condition that the fuel cell output is 55V and 1kW grid-connected operating conditions. It can be seen that the current ripple control method for reducing the ripple of the dc-link capacitor on the output side is applied so that the current ripple on the fuel cell side is significantly increased to about 25%. Fig. 26(b) shows the characteristics of the proposed power converter under the condition that the input voltage of the fuel cell is 55V

and 1kW. The converter output dc voltage is controlled at 420V, and the fuel cell output current waveform is controlled with a constant current. The inverter output voltage and current waveform confirm a suitable grid connection status. The power factor is 99.98%, and THD (Total harmonics distortion) is 3.8% up to the 50<sup>th</sup> order. Fig. 26(c) shows the fuel cell output current ripple under the 1kW output condition.  $i_f$  is the output current of the fuel cell is about 20A.  $i_f$  is the ripple waveform measured using the AC mode of the oscilloscope. The peak value of the fuel cell output current source is about 1A, and there is a current ripple of 120Hz. This value corresponds to a current ripple of 5%.

Fig. 27 is the result of testing the starting and stopping characteristics of the system in an independent operation state to verify the dynamic features of the proposed fuel cell power generation system. At this time, the fuel cell current ripple is controlled by 5%. Fig. 27(a) represents the starting characteristics of the system under the rated load condition. It can be seen that the soft start operation of about 0.18s before turning on the MC quickly makes it to a steady state without overshooting even under the rated load condition. Fig. 27(b) shows the stopping characteristics of the system under the rated load condition. When the MC is turned off, it can be

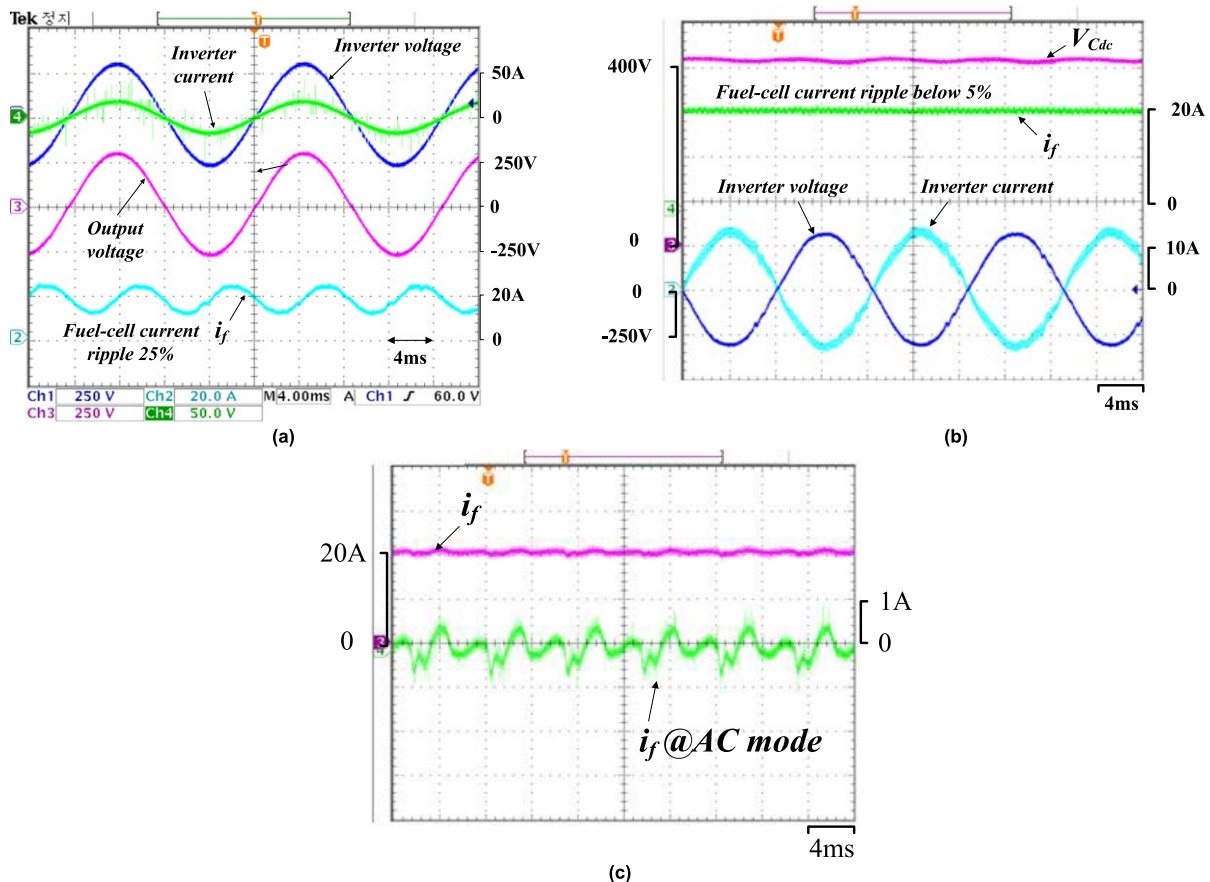


**FIGURE 26.** Fuel cell current ripple, inverter voltage, and inverter current according to the ripple control method, (a) current ripple control, 25% current ripple, (b) voltage ripple control, current ripple 5% below, (c) fuel cell current ripple using the AC mode of the oscilloscope.

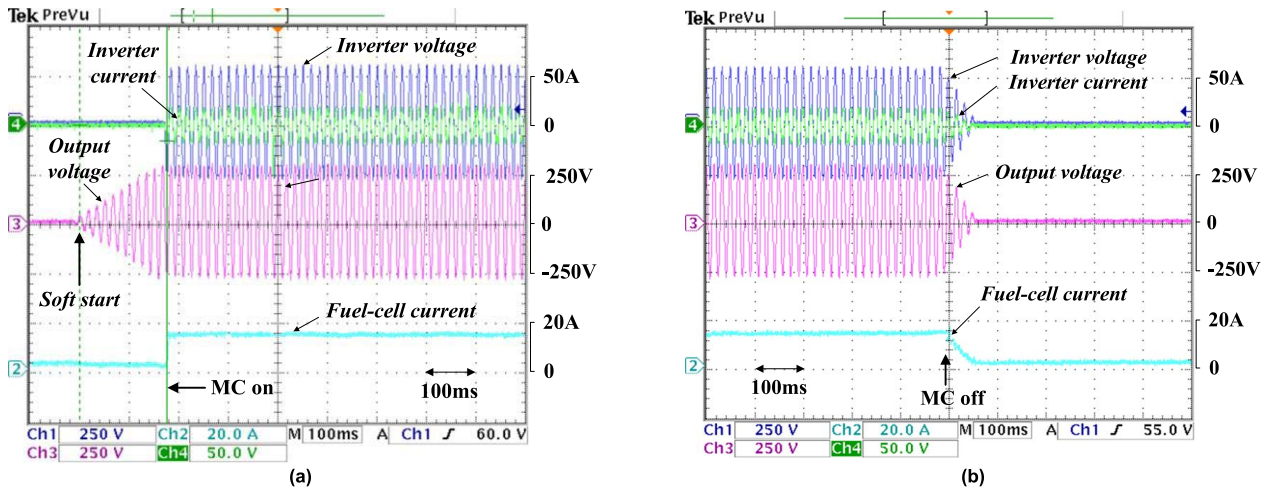


FIGURE 27. Dynamic characteristics of the proposed system at rated load conditions, (a) at starting, (b) at stopping.

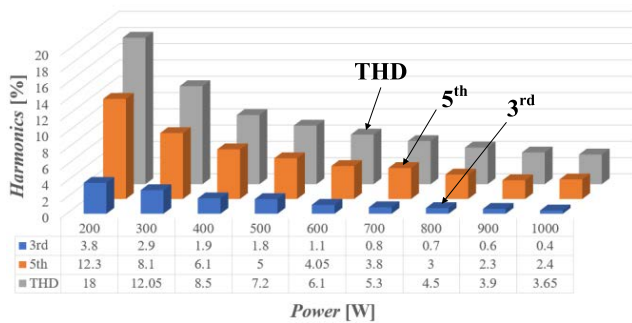


FIGURE 28. 3<sup>rd</sup> and 5<sup>th</sup> harmonics and THD analysis up to 50<sup>th</sup> order according to fuel cell output when the grid is connected.

seen that the output voltage is stably reduced along with the reduction of the fuel cell power generation.

Fig. 28 results from analyzing the 3<sup>rd</sup> harmonic, 5<sup>th</sup> harmonic, and THD when the current harmonics were measured up to 50<sup>th</sup> order according to the fuel cell output when the grid is connected.

The 3<sup>rd</sup> harmonic, 5<sup>th</sup> harmonic, and THD become more significant as the load is lower and smaller as the output increases. At 200W, the 3<sup>rd</sup> harmonic component was about 3.8%, the 5<sup>th</sup> harmonic component was about 12.3%, and the THD was about 18%. At the rated load of 1kW, the 3<sup>rd</sup> harmonic component was about 0.4%, the 5<sup>th</sup> harmonic component was about 2.4%, and the THD was about 3.65%, which is good. In the grid-connected inverter, the 3<sup>rd</sup> and 5<sup>th</sup> harmonic components are 3% or less, and the THD is regulated as 5% or less, which is satisfactory.

Fig. 29 shows the results of comparing the efficiency of the proposed method with the fuel cell system using the conventional hard-switching current-type push-pull converter. At the fuel cell output voltage of 55V, the traditional way showed a minimum efficiency of about 85.1% at 1,000W, and the maximum efficiency was approximately 86.7% at 600W. The proposed method showed about 88.4% when

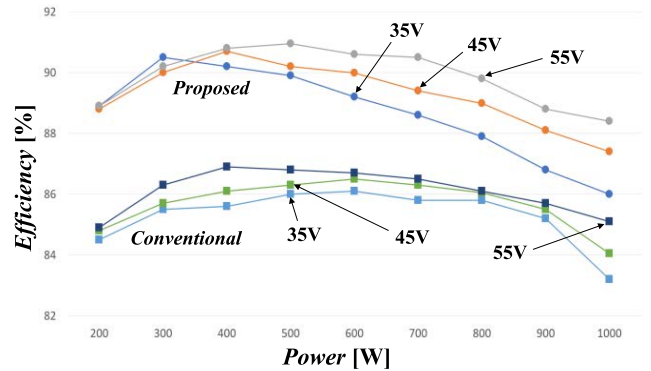


FIGURE 29. Efficiency comparison between the case of applying the conventional push-pull converter and the case of applying the proposed converter at the fuel cell output voltages 35V, 45V, and 55V.

outputting 1,000W and about 90.95% when outputting 500W was excellent. At 500W, which is half of the rating, the maximum efficiency of the fuel cell power conversion system is shown, the efficiency of the grid-connected inverter is about 97%, and the efficiency of the proposed converter is about 91%, so the total efficiency of the system is measured to be about 94%.

Factors affecting power loss in the proposed converter system can be roughly divided into four categories. First, switch loss ( $P_s$ ) is subdivided into switching loss that occurs during turn-on and turn-off of the switch ( $P_T$ ), conduction loss due to  $R_{on}$  resistance of the switch ( $P_{on}$ ), and gate driving loss ( $P_D$ ).

$$P_s = P_{on} + P_T + P_D \quad (35)$$

Here, conduction loss is defined as

$$P_{on} = I_{Qx,rms}^2 R_{DS,on} \quad (36)$$

where  $I_{Qx,rms}$  is the RMS current flowing through the switch, and  $R_{DS,on}$  is the switch on resistance.



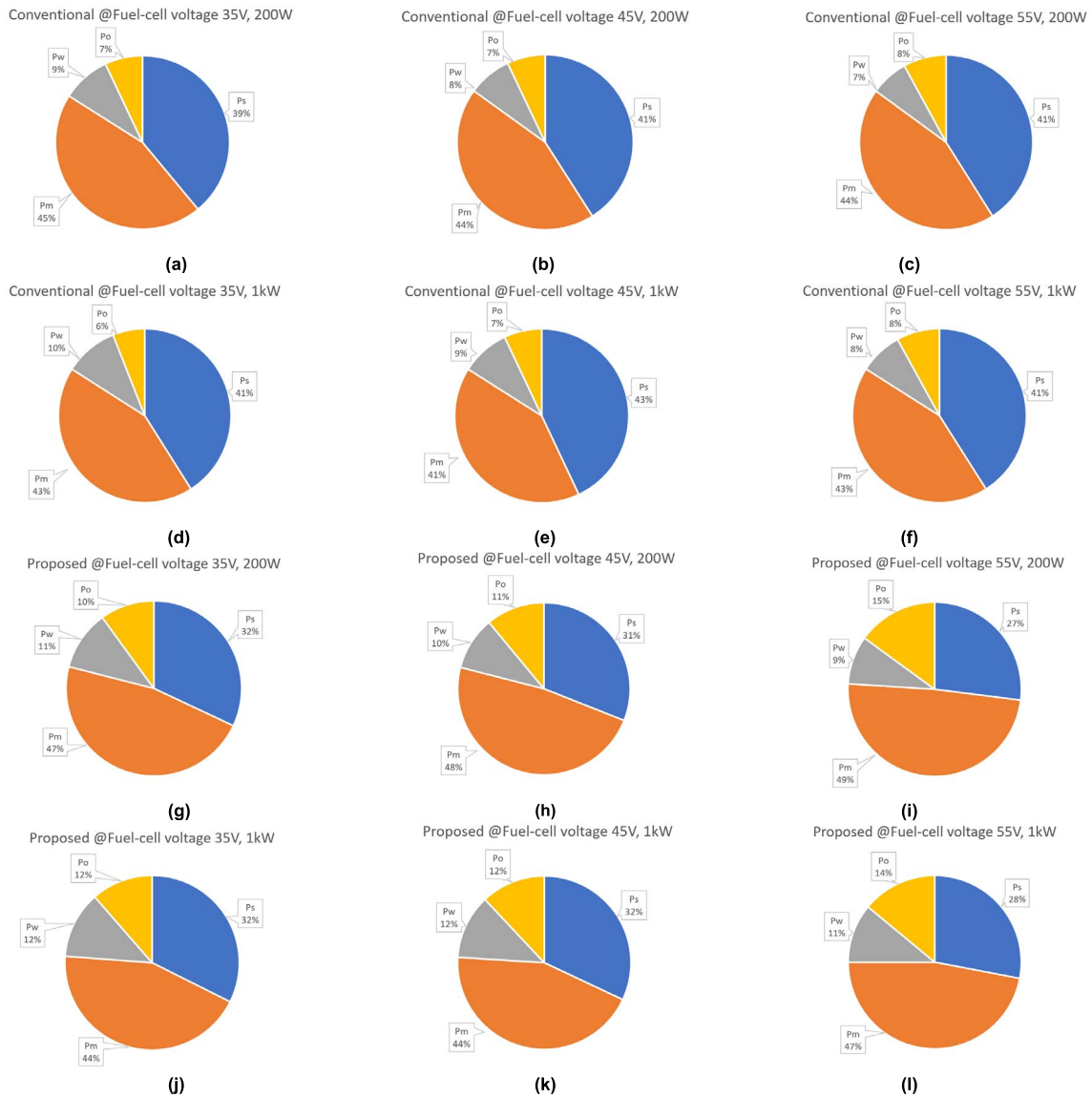


**FIGURE 30.** Power loss breakdown for the traditional push-pull converter and the proposed approach with the fuel cell voltage of 35V, 45V, and 55V at 200W and 1kW, (a) conventional @ fuel cell voltage 35V, 200W, (b) conventional @ fuel cell voltage 45V, 200W, (c) conventional @ fuel cell voltage 55V, 200W, (d) conventional @ fuel cell voltage 35V, 1kW, (e) conventional @ fuel cell voltage 45V, 1kW, (f) conventional @ fuel cell voltage 55V, 1kW, (g) proposed @ fuel cell voltage 35V, 200W, (h) proposed @ fuel cell voltage 45V, 200W, (i) proposed @ fuel cell voltage 55V, 200W, (j) proposed @ fuel cell voltage 35V, 1kW, (k) proposed @ fuel cell voltage 45V, 1kW, (l) proposed @ fuel cell voltage 55V, 1kW.

The switching losses that occur during switch turn-on ( $P_{SW,on}$ ), and turn-off ( $P_{SW,off}$ ), are expressed as follows.

$$P_T = P_{SW,on} + P_{SW,off} = \frac{1}{T_{sw}} \left( \int_0^{tr} v_{DS} i_D dt + \int_{tr}^{tr+tw} v_{DS} i_D dt \right) \quad (37)$$

The integration period  $tr$  is a period in which the current completely falls from the peak to zero when the switch is turned off.  $tw$  is the period in which the current flows through the switch. In the proposed converter, the push-pull switch can perform soft switching at any switch on-off moment, but in the buck converter switch, ZVS occurs only during switch turn-off, so switching loss occurs at the turn-on moment.

The gate driving loss ( $P_D$ ) is expressed as

$$P_{D,on} = P_{D,off} = \frac{1}{2} (Q_{GS} \cdot f_s \cdot V_{gs}) \quad (38)$$

where  $Q_{GS}$  is the gate-source charge,  $f_s$  is the switching frequency, and  $V_{gs}$  is the gate-source voltage.

Second, core loss and copper loss occur due to the transformer and inductor. The transformer and inductor use EPCOS PM87/70(N27) core in the prototype. The EPCOS core has a very high magnetic permeability compared to a general core and has excellent frequency characteristics. It is possible to design a transformer with a low number of turns for high output due to high permeability, thereby minimizing copper loss, and designing a transformer with low leakage

inductance and parasitic capacitance.

$$P_m = P_{fe} + P_{cu} \quad (39)$$

$$P_{cu} = \left( \frac{\rho \lambda_1^2 I_{tot}^2}{4K_u} \right) \left( \frac{MLT}{W_A A_c^2} \right) \left( \frac{1}{B_{max}} \right)^2 \quad (40)$$

$$P_{fe} = K_{fe} (B_{max})^\beta A_c l_m \quad (41)$$

$$\text{where } B_{max} = \left( \frac{\rho \lambda_1^2 I_{tot}^2}{2K_u} \cdot \frac{MLT}{W_A A_c^2 l_m} \cdot \frac{1}{\beta K_{fe}} \right)^{\frac{1}{\beta+2}}.$$

Here,  $P_{cu}$  is total copper loss.  $P_{fe}$  is total core loss.  $\rho$  is the effective resistivity of a wire.  $\lambda_1$  is the primary flux linkage.  $I_{tot}$  is total RMS winding current referred to primary of the transformer.  $K_u$  is the Winding fill factor. MLT is the mean length per turn.  $W_A$  is the core window area.  $A_c$  is the core cross-sectional area.  $B_{max}$  is peak AC flux density.  $l_m$  is the magnetic path length.  $K_{fe}$  is the core loss coefficient.  $\beta$  is the core loss exponent.

Third, it is a copper loss due to a wire loss of about 1.5 m for the connection between the fuel cell and the converter system.

$$P_w = R_{wire} I_o^2 \quad (42)$$

where  $R_{wire}$  is the total resistance of wires between the fuel cell and the proposed system, and  $I_o$  is the dc-output current.

Fourth, the loss that cannot be accurately distinguished is ohmic loss due to low parasitic inductance of PCB, internal loss of capacitor, Litz-wire cooper loss of magnetic components due to skin effect or proximity effect, and ohmic loss due to switch and magnetic material due to increase in operating temperature [66], [67], [68], [69], [70].  $P_o$  is obtained by subtracting ( $P_s + P_m + P_w$ ) from the efficiency value obtained from the actual measurement ( $P_{measured}$ ) in Fig. 29.

$$P_o = P_{measured} - (P_s + P_m + P_w) \quad (43)$$

Fig. 30 shows the power loss analysis results of the conventional push-pull converter and the proposed method. Among the measured efficiency data in Fig. 29, we analyze the loss when the fuel cell voltage is 35V, 45V, and 55V at 200W and 1kW. In both the proposed and existing methods, the loss due to the magnetic material ( $P_m$ ) and the loss component due to the switch ( $P_s$ ) appear the largest. Existing push-pull converters have significant switching losses due to hard switching. On the other hand, the proposed method has a relatively small switching loss due to the ZVS operation. However, it shows that the power loss component due to the magnetic material is significant. When designing a transformer, which is a factor that significantly affects the efficiency of this converter system, it is necessary to consider the total handling power, which is the product of the operating voltage and the maximum current, and the minimum operational efficiency and maximum allowable temperature due to the maximum loss. In addition, it is necessary to design a core considering trade-offs such as weight, economy, and volume, such as selecting appropriate material and a size suitable for the operating frequency. However, in the case of laboratory-level prototypes, the optimal efficiency was not achieved by

selecting a core with a similar value that was easily obtained rather than the calculated optimal core.

#### IV. CONCLUSION

We proposed a grid connection method using a structure that can reduce the low-frequency ripple component of the fuel cell output current by combining a buck converter and a push-pull converter. Although the proposed dc-to-dc converter has a two-stage structure, it has the same number of inductors as the single-stage method, and the capacitor, an intermediate voltage source, can be removed. The peak current of the push-pull converter was reduced by designing a high-frequency transformer to enable rated output even at the lowest output value of the fuel cell and operating the buck converter at twice the switching frequency of the push-pull converter. In addition, a new method of charging the battery by controlling the amount of oxygen in the fuel cell system without using a charger was proposed.

The ZVS and ZCS operations were verified through simulations and experiments, and it was confirmed that the low-frequency current ripple of the fuel cell was maintained within 5%. The THD of the grid current at 800W or higher was maintained at 5% or less when connecting to the grid. At 500W, the fuel cell power conversion system shows the maximum efficiency, the efficiency of the grid-connected inverter is about 97%, and the efficiency of the proposed converter is about 91%. Therefore, the overall efficiency of the grid-connected system was measured to be about 94%.

#### REFERENCES

- [1] L. Sun, Y. Jin, L. Pan, J. Shen, and K. Y. Lee, "Efficiency analysis and control of a grid-connected PEM fuel cell in distributed generation," *Energy Convers. Manage.*, vol. 195, pp. 587–596, Sep. 2019.
- [2] C. Weyers and T. Bocklisch, "Simulation-based investigation of energy management concepts for fuel cell–battery–hybrid energy storage systems in mobile applications," *Energy Proc.*, vol. 155, pp. 295–308, Nov. 2018.
- [3] M. R. Mahmud and H. R. Pota, "Robust nonlinear controller design for DC–AC converter in grid-connected fuel cell system," *IEEE J. Emerg. Sel. Topics Ind. Electron.*, vol. 3, no. 2, pp. 342–351, Apr. 2022.
- [4] J. Kim, J. Lee, and B. H. Cho, "Equivalent circuit modeling of PEM fuel cell degradation combined with a LFRC," *IEEE Trans. Ind. Electron.*, vol. 60, no. 11, pp. 5086–5094, Nov. 2013.
- [5] C. Liu and J.-S. Lai, "Low frequency current ripple reduction technique with active control in a fuel cell power system with inverter load," *IEEE Trans. Power Electron.*, vol. 22, no. 4, pp. 1429–1436, Apr. 2007.
- [6] X. Liu, H. Li, and Z. Wang, "A fuel cell power conditioning system with low-frequency ripple-free input current using a control-oriented power pulsation decoupling strategy," *IEEE Trans. Power Electron.*, vol. 29, no. 1, pp. 159–169, Jan. 2014.
- [7] J. Itoh and F. Hayashi, "Ripple current reduction of a fuel cell for a single phase isolated converter using a DC active filter with a center tap," *IEEE Trans. Power Electron.*, vol. 25, no. 3, pp. 550–556, Mar. 2010.
- [8] R. S. Gemmen, "Analysis for the effect of inverter ripple current on fuel cell operation condition," *J. Fluid Mech.*, vol. 125, no. 3, pp. 576–585, Jun. 2003.
- [9] P. Wang, L. Zhou, Y. Zhang, J. Li, and M. Sumner, "Input-parallel output-series DC–DC boost converter with a wide input voltage range, for fuel cell vehicles," *IEEE Trans. Veh. Technol.*, vol. 66, no. 9, pp. 7771–7781, Sep. 2017.
- [10] M. Inci and Ö. Türksöy, "Review of fuel cells to grid interface: Configurations, technical challenges and trends," *J. Cleaner Prod.*, vol. 213, pp. 1353–1370, Mar. 2019.

- [11] R.-J. Wai and C.-Y. Lin, "Active low-frequency ripple control for clean-energy power-conditioning mechanism," *IEEE Trans. Ind. Electron.*, vol. 57, no. 11, pp. 3780–3792, Nov. 2010.
- [12] K. R. Sekhar and S. Srinivas, "Discontinuous decoupled PWMs for reduced current ripple in a dual two-level inverter fed open-end winding induction motor drive," *IEEE Trans. Power Electron.*, vol. 28, no. 5, pp. 2493–2502, May 2013.
- [13] Y. Ohnuma, K. Orikawa, and J. Itoh, "A single-phase current source PV inverter with power decoupling capability using an active buffer," *IEEE Trans. Ind. Appl.*, vol. 51, no. 1, pp. 531–538, Jan./Feb. 2015.
- [14] J. Wang, B. Ji, X. Lu, X. Deng, F. Zhang, and C. Gong, "Steady-state and dynamic input current low-frequency ripple evaluation and reduction in two-stage single-phase inverters with back current gain model," *IEEE Trans. Power Electron.*, vol. 29, no. 8, pp. 4247–4260, Aug. 2014.
- [15] M. Saito and N. Matsui, "Modeling and control strategy for a single-phase PWM rectifier using a single-phase instantaneous active/reactive power theory," in *Proc. 25th Int. Telecommun. Energy Conf.*, Oct. 2003, pp. 573–578.
- [16] J. Kan, S. Xie, Y. Wu, Y. Tang, Z. Yao, and R. Chen, "Single-stage and boost-voltage grid-connected inverter for fuel-cell generation system," *IEEE Trans. Ind. Electron.*, vol. 62, no. 9, pp. 5480–5490, Sep. 2015.
- [17] M. Forouzesh, Y. P. Siwakoti, S. A. Gorji, F. Blaabjerg, and B. Lehman, "Step-up DC–DC converters: A comprehensive review of voltage-boosting techniques, topologies, and applications," *IEEE Trans. Power Electron.*, vol. 32, no. 12, pp. 9143–9178, Dec. 2017.
- [18] Y.-T. Chen, Z.-X. Lu, and R.-H. Liang, "Analysis and design of a novel high-step-up DC/DC converter with coupled inductors," *IEEE Trans. Power Electron.*, vol. 33, no. 1, pp. 425–436, Jan. 2018.
- [19] L. He, Z. Lin, Q. Tan, F. Lu, and T. Zeng, "Interleaved high step-up current sharing converter with coupled inductors," *Electron*, vol. 10, no. 4, pp. 1–14, 2021.
- [20] X. Hu, J. Wang, L. Li, and Y. Li, "A three-winding coupled-inductor DC–DC converter topology with high voltage gain and reduced switch stress," *IEEE Trans. Power Electron.*, vol. 33, no. 2, pp. 1453–1462, Feb. 2018.
- [21] M. Nguyen, T. Duong, and Y. Lim, "Switched-capacitor-based dual-switch high-boost DC–DC converter," *IEEE Trans. Power Electron.*, vol. 33, no. 5, pp. 4181–4189, May 2018.
- [22] L. Yang, W. Yu, and J. Zhang, "High voltage gain ratio isolated resonant switched-capacitor converter for sustainable energy," *IEEE Access*, vol. 7, pp. 23055–23067, 2019.
- [23] G. Wu, X. Ruan, and Z. Ye, "High step-up DC–DC converter based on switched capacitor and coupled inductor," *IEEE Trans. Ind. Electron.*, vol. 65, no. 7, pp. 5572–5579, Jul. 2018.
- [24] H. Ardi, A. Ajami, and M. Sabahi, "A novel high step-up DC–DC converter with continuous input current integrating coupled inductor for renewable energy applications," *IEEE Trans. Ind. Electron.*, vol. 65, no. 2, pp. 1306–1315, Feb. 2018.
- [25] M. A. Salvador, T. B. Lazzarin, and R. F. Coelho, "High step-up DC–DC converter with active switched-inductor and passive switched-capacitor networks," *IEEE Trans. Ind. Electron.*, vol. 65, no. 7, pp. 5644–5654, Jul. 2018.
- [26] S. Hasanpour, M. Forouzesh, and A. Novel, "Full soft-switching high gain DC/DC converter based on three-winding coupled-inductor," *IEEE Trans. Power Electron.*, vol. 36, no. 11, pp. 12656–12669, Apr. 2021.
- [27] L. Mitra and U. K. Rout, "Comparative study of multi-stage boost converter for high voltage and high power applications," in *Proc. 19th OITS Int. Conf. Inf. Technol. (OCIT)*, Bhubaneswar, India, Dec. 2021, pp. 422–427.
- [28] A. Mostaan, J. Yuan, Y. P. Siwakoti, S. Esmaili, and F. Blaabjerg, "A trans-inverse coupled-inductor semi-SEPIC DC/DC converter with full control range," *IEEE Trans. Power Electron.*, vol. 34, no. 11, pp. 10398–10402, Nov. 2019.
- [29] J. Yuan, A. Mostaan, Y. Yang, Y. P. Siwakoti, and F. Blaabjerg, "A modified Y-source DC–DC converter with high voltage-gains and low switch stresses," *IEEE Trans. Power Electron.*, vol. 35, no. 8, pp. 7716–7720, Aug. 2020.
- [30] R. Rahimi, S. Habibi, P. Shamsi, and M. Ferdowsi, "A high step-up Z-source DC–DC converter for integration of photovoltaic panels into DC microgrid," in *Proc. IEEE Appl. Power Electron. Conf. Expo. (APEC)*, Jun. 2021, pp. 1416–1420.
- [31] R. Rahimi, S. Habibi, M. Ferdowsi, and P. Shamsi, "A two-phase interleaved high-voltage gain DC–DC converter with coupled inductor and built-in transformer for photovoltaic applications," in *Proc. 47th Annu. Conf. IEEE Ind. Electron. Soc. (IECON)*, Oct. 2021, pp. 1–6.
- [32] M. Prudente, L. L. Pfitscher, G. Emmendoerfer, E. F. Romaneli, and R. Gules, "Voltage multiplier cells applied to non-isolated DC–DC converters," *IEEE Trans. Power Electron.*, vol. 23, no. 2, pp. 871–887, Mar. 2008.
- [33] R. Rahimi, S. Habibi, M. Ferdowsi, and P. Shamsi, "Z-source-based high step-up DC–DC converters for photovoltaic applications," *IEEE J. Emerg. Sel. Topics Power Electron.*, vol. 10, no. 4, pp. 1–14, Aug. 2021.
- [34] B. P. Baddipadiga and M. Ferdowsi, "A high-voltage-gain DC–DC converter based on modified Dickson charge pump voltage multiplier," *IEEE Trans. Power Electron.*, vol. 32, no. 10, pp. 7707–7715, Oct. 2017.
- [35] R. Rahimi, S. Habibi, P. Shamsi, and M. Ferdowsi, "An interleaved high step-up DC–DC converter based on combination of coupled inductor and built-in transformer for photovoltaic-grid electric vehicle DC fast charging systems," in *Proc. IEEE Texas Power Energy Conf. (TPEC)*, Feb. 2021, pp. 1–6.
- [36] R. Rahimi, S. Habibi, M. Ferdowsi, and P. Shamsi, "A three-winding coupled inductor-based interleaved high-voltage gain DC–DC converter for photovoltaic systems," *IEEE Trans. Power Electron.*, vol. 37, no. 1, pp. 990–1002, Jan. 2022.
- [37] S.-G. Song, F.-S. Kang, S.-J. Park, C.-J. Moon, and G.-J. Son, "Zero-voltage and zero-current switched fuel-cell powered DC-to-DC converter," in *Proc. Int. Symp. Signals, Circuits Syst., Iasi, Romania*, Jul. 2007, pp. 13–14.
- [38] Q. Tong, N. Zhong, M. Yang, and D. Zhang, "A ZVS DC–DC converter based on buck topology," in *Proc. IEEE Int. Conf. Intell. Appl. Syst. Eng. (ICIASE)*, Fuzhou, China, Apr. 2019, pp. 26–29.
- [39] Q. Tong, N. Zhong, M. Yang, and D. Zhang, "A ZVS buck converter with fixed frequency control," in *Proc. 14th IEEE Conf. Ind. Electron. Appl. (ICIEA)*, Xi'an, China, Jun. 2019, pp. 19–21.
- [40] M. Kumar, M. Pattnaik, and J. Mishra, "An improved ZVS-PWM buck converter with ZCS auxiliary circuit," in *Proc. IEEE Region 10th Conf. (TENCON)*, Penang, Malaysia, Nov. 2017, pp. 5–8.
- [41] G. Moschopoulos, P. K. Jain, Y.-F. Liu, and G. Joos, "A zero-voltage-switched PWM boost converter with an energy feedforward auxiliary circuit," *IEEE Trans. Power Electron.*, vol. 14, no. 4, pp. 653–662, Jul. 1999.
- [42] S. Chattopadhyay, S. Baratam, and H. Agrawal, "A new family of active clamp PWM DC–DC converters with ZVS for main switch and ZCS for auxiliary switch," in *Proc. 26th Annu. IEEE Appl. Power Electron. Conf. Expo. (APEC)*, Mar. 2011, pp. 851–858.
- [43] N. Lakshminarasamma, B. Swaminathan, and V. Ramanarayanan, "A unified model for the ZVS DC–DC converters with active clamp," in *Proc. IEEE 35th Annu. Power Electron. Spec. Conf.*, Jun. 2004, pp. 2441–2447.
- [44] A. Ali and Y. Liao, "Optimized control for modified push-pull dual active bridge converter to achieve wide ZVS range and low current stress," *IEEE Access*, vol. 9, pp. 140258–140267, 2021.
- [45] L. Jiang, J. Wan, Y. Li, C. Huang, F. Liu, H. Wang, Y. Sun, and Y. Cao, "A new push-pull DC/DC converter topology with complementary active clamped," *IEEE Trans. Ind. Electron.*, vol. 69, no. 6, pp. 6445–6449, Jun. 2022.
- [46] K. Yamamoto, E. Hiraki, T. Tanaka, M. Nakaoka, and T. Mishima, "Bidirectional DC–DC converter with full-bridge/ push-pull circuit for automobile electric power systems," in *Proc. 37th IEEE Power Electron. Spec. Conf.*, Jun. 2006, pp. 1–5.
- [47] E. Hiraki, K. Hirao, T. Tanaka, and T. Mishima, "A push-pull converter based bidirectional DC–DC interface for energy storage systems," in *Proc. 13th Eur. Conf. Power Electron. Appl.*, Sep. 2009, pp. 1–10.
- [48] Y. Lu, Q. Wu, Q. Wang, D. Liu, and L. Xiao, "Analysis of a novel zero-voltage-switching bidirectional DC/DC converter for energy storage system," *IEEE Trans. Power Electron.*, vol. 33, no. 4, pp. 3169–3179, Apr. 2018.
- [49] T.-T. Le, S. Kim, and S. Choi, "A four-phase current-fed push-pull DAB converter for wide-voltage-range applications," *IEEE Trans. Power Electron.*, vol. 36, no. 10, pp. 11383–11396, Oct. 2021.
- [50] Z. Zhang, O. C. Thomsen, and M. A. E. Andersen, "Optimal design of a push-pull-forward half-bridge (PPFHB) bidirectional DC–DC converter with variable input voltage," *IEEE Trans. Ind. Electron.*, vol. 59, no. 7, pp. 2761–2771, Jul. 2012.

- [51] L. Sun, Y. Jin, L. Pan, J. Shen, and K. Y. Lee, "Efficiency analysis and control of a grid-connected PEM fuel cell in distributed generation," *Energy Convers. Manage.*, vol. 195, pp. 587–596, Sep. 2019.
- [52] A. B. Shitole, S. Sathyan, H. M. Suryawanshi, G. G. Talapur, and P. Chaturvedi, "Soft-switched high voltage gain boost-integrated flyback converter interfaced single-phase grid-tied inverter for SPV integration," *IEEE Trans. Ind. Appl.*, vol. 54, no. 1, pp. 482–493, Jan. 2017.
- [53] M. Kumar, K. Mathuriya, V. K. Yadav, and A. K. Verma, "Soft switched high gain boost converter for low voltage applications," in *Proc. IEEE Energy Convers. Congr. Expo. (ECCE)*, Vancouver, BC, Canada, Oct. 2021, pp. 10–14.
- [54] F. S. Al-Ismael, "DC microgrid planning, operation, and control: A comprehensive review," *IEEE Access*, vol. 9, pp. 36154–36172, 2021.
- [55] V. K. Goyal and A. Shukla, "Isolated DC–DC boost converter for wide input voltage range and wide load range applications," *IEEE Trans. Ind. Electron.*, vol. 68, no. 10, pp. 9527–9539, Oct. 2021.
- [56] S. Neira, J. Pereda, and F. Rojas, "Three-port full-bridge bidirectional converter for hybrid DC/DC/AC systems," *IEEE Trans. Power Electron.*, vol. 35, no. 12, pp. 13077–13084, Dec. 2020.
- [57] P. Xuewei and A. K. Rathore, "Novel bidirectional snubberless naturally commutated soft-switching current-fed full-bridge isolated DC/DC converter for fuel cell vehicles," *IEEE Trans. Ind. Electron.*, vol. 61, no. 5, pp. 2307–2315, May 2014.
- [58] B. Han, C. Bai, J. S. Lee, and M. Kim, "Repetitive controller of capacitorless current-fed dual-half-bridge converter for grid-connected fuel cell system," *IEEE Trans. Power Electron.*, vol. 65, no. 10, pp. 7841–7855, Oct. 2018.
- [59] X. Pan, H. Li, Y. Liu, T. Zhao, C. Ju, and A. K. Rathore, "An overview and comprehensive comparative evaluation of current-fed-isolated-bidirectional DC/DC converter," *IEEE Trans. Power Electron.*, vol. 35, no. 3, pp. 2737–2763, Mar. 2020.
- [60] H. Moradisizkoochi, N. Elsayad, and O. A. Mohammed, "Experimental verification of a double-input soft-switched DC–DC converter for fuel cell electric vehicle with hybrid energy storage system," *IEEE Trans. Ind. Appl.*, vol. 55, no. 6, pp. 6451–6465, Nov. 2019.
- [61] H. Moradisizkoochi, N. Elsayad, and O. A. Mohammed, "A family of three-port three-level converter based on asymmetrical bidirectional half-bridge topology for fuel cell electric vehicle applications," *IEEE Trans. Power Electron.*, vol. 34, no. 12, pp. 11706–11724, Dec. 2019.
- [62] Q. Wu, Q. Wang, J. Xu, H. Li, and L. Xiao, "A high-efficiency step-up current-fed push-pull quasi-resonant converter with fewer components for fuel cell application," *IEEE Trans. Ind. Electron.*, vol. 64, no. 8, pp. 6639–6648, Aug. 2017.
- [63] S. Lee, J. Park, and S. Choi, "A three-phase current-fed push-pull DC–DC converter with active clamp for fuel cell applications," *IEEE Trans. Power Electron.*, vol. 26, no. 8, pp. 2266–2277, Aug. 2011.
- [64] Q. Wu, Q. Wang, J. Xu, and L. Xiao, "Implementation of an active-clamped current-fed push-pull converter employing parallel-inductor to extend ZVS range for fuel cell application," *IEEE Trans. Ind. Electron.*, vol. 64, no. 10, pp. 7919–7929, Oct. 2017.
- [65] J.-M. Kwon, E.-H. Kim, B.-H. Kwon, and K.-H. Nam, "High-efficiency fuel cell power conditioning system with input current ripple reduction," *IEEE Trans. Ind. Electron.*, vol. 56, no. 3, pp. 826–834, Mar. 2009.
- [66] S. Inoue and H. Akagi, "A bidirectional DC–DC converter for an energy storage system with galvanic isolation," *IEEE Trans. Power Electron.*, vol. 22, no. 6, pp. 2299–2306, Nov. 2007.
- [67] N. Perera, R. V. Erp, J. Ancay, A. Jafari, and E. Matioli, "Active-device losses in resonant power converters: A case study with class-E inverters," in *Proc. IEEE Energy Convers. Congr. Expo. (ECCE)*, Oct. 2021, pp. 5312–5319.
- [68] G.-C. Huang, T.-J. Liang, and K.-H. Chen, "Losses analysis and low standby losses quasi-resonant flyback converter design," in *Proc. IEEE Int. Symp. Circuits Syst. (ISCAS)*, May 2012, pp. 217–220.
- [69] R. Haneda and H. Akagi, "Power-loss characterization and reduction of the 750-V 100-KW 16-KHz dual-active-bridge converter with buck and boost mode," *IEEE Trans. Ind. Appl.*, vol. 58, no. 1, pp. 541–553, Jan. 2022.
- [70] R. W. Erickson, *Fundamentals of Power Electronics*, 2nd ed. New York, NY, USA: Springer, 2001, pp. 565–586.



**GYOUNG-JONG SON** received the B.S. degree in electronic engineering from Chosun University, Gwangju, South Korea, in 1988, and the M.S. and Ph.D. degrees in electrical engineering from Chonnam National University, Gwangju, in 2003 and 2007, respectively.

Since 2003, he has been working at Gwangju Metropolitan City. In 2013, he was the Director of the Strategic Industry Division, Bureau of Economy, Trade and Industry, Gwangju Metropolitan City. In 2014, he served as the Director of Automobile Industry Division, Economic and Industrial Bureau, Gwangju Metropolitan City. In 2016, he served as the Director of the Automobile Industry Division, Strategic Industry Bureau, Gwangju Metropolitan City. In 2017, he was the Director-General of the Employment and Economy Bureau, Gwangju Metropolitan City. In 2018, he was the Director-General of Strategic and Industries, Gwangju Metropolitan City. Since 2020, he has been the Director-General of the Artificial Intelligence Industry, Gwangju Metropolitan City. Since 2022, he has been an Invited Research Fellow with the Department of Electrical Engineering, Chonnam National University. His research interests include power electronics, fuel-cell-powered system design, and control.



**FEEL-SOON KANG** (Member, IEEE) received the B.S. degree in electrical engineering from Gyeongsang National University, South Korea, in 1998, and the M.S. and Ph.D. degrees in electrical engineering from Pusan National University, South Korea, in 2000 and 2003, respectively. Since 2003, he has been a Postdoctoral Fellow with the Department of Electrical Engineering, Osaka University, Japan. From 2004 to 2022, he was a Professor with the Department of Electronic Engineering, Hanbat National University, Daejeon, South Korea. Since 2022, he has been a Professor with the Department of Mechatronics Engineering, Gyeongsang National University. His research interests include power electronics, design, control, and reliability analysis of various power conversion systems for photovoltaic power generation, electric vehicles, and HVDC systems. He is a member of KIEE and KIPE. He received the Student Award and the Best Presentation Prizes from the IEEE Industrial Electronics Society, in 2001, and he was honored with Academic Awards from Pusan National University and Hanbat National University in 2003 and 2005, respectively. He also received several Best Paper Awards from The Korean Institute of Electrical Engineers (KIEE) and The Korean Institute of Power Electronics (KIPE). He was the Vice-Chairman of the Organizing Committee for the International Telecommunications Energy Conference (IEEE Intelec 2009), IEEE Vehicle Power and Propulsion Conference (IEEE VPPC 2012), IEEE Transportation Electrification Conference and Expo (IEEE ITEC 2016), International Conference on Electrical Machines and Systems (ICEMS 2010, 2013, and 2018) and the Secretary of International Conference on Magnetically Levitated Systems and Linear Drives (Maglev 2011). He was an Associate Editor of the IEEE TRANSACTIONS ON INDUSTRIAL ELECTRONICS, from 2004 to 2011.

Since 2003, he has been a Professor with the Department of Electrical Engineering, Chonnam National University, Gwangju, South Korea. His research interests include power electronics, motor control, mechatronics, and micromachine automation. He has been the President of The Korean Society of Industry Convergence since 2019. He is a member of KIEE, KIPE, and KIIEE.



**SUNG-JUN PARK** received the B.S., M.S., and Ph.D. degrees in electrical engineering and the Ph.D. degree in mechanical engineering from Pusan National University, Busan, South Korea, in 1991, 1993, 1996, and 2002, respectively. From 1996 to 2000, he was an Assistant Professor at the Department of Electrical Engineering, Koje College, Koje, South Korea. From 2000 to 2003, he was an Assistant Professor at the Department of Electrical Engineering, Tongmyong College, Busan. Since 2003, he has been a Professor with the Department of Electrical Engineering, Chonnam National University, Gwangju, South Korea. His research interests include power electronics, motor control, mechatronics, and micromachine automation. He has been the President of The Korean Society of Industry Convergence since 2019. He is a member of KIEE, KIPE, and KIIEE.